TITLE: Mapping human serum induced gene networks as a basis for the creation of biomimetic periosteum for bone repair

AUTHORS: Rawiya Al Hosni, Mittal Shah, Umber Cheema, Helen C. Roberts, Frank P. Luyten and Scott J. Roberts

JOURNAL: Cytotherapy

PUBLISHER: Elsevier

PUBLICATION DATE: 7 June 2020

DOI: https://doi.org/10.1016/j.jcyt.2020.03.434

Mapping human serum induced gene networks as a basis for the creation of biomimetic periosteum for bone repair

Rawiya Al Hosni[1], Mittal Shah[1], Umber Cheema[1], Helen C. Roberts[2], Frank P. Luyten[3] and Scott J. Roberts[1,3,4]*

[1]Department of Materials and Tissue, Institute of Orthopaedics and Musculoskeletal Science, University College London, Stanmore, UK.

[2] Department of Natural Sciences, Faculty of Science & Technology, Middlesex University, London, UK.

[3]Skeletal Biology and Tissue Engineering Centre, Department of Development and Regeneration, KU Leuven, Leuven, Belgium.

[4]Department of Comparative Biomedical Sciences, The Royal Veterinary College, London, UK

*Corresponding Author: Dr. Scott J. Roberts

Department of Comparative Biomedical Sciences, The Royal Veterinary College, London, UK

sjroberts@rvc.ac.uk

Keywords: periosteum, bone defect, periosteal cells, transcriptomics, cell potency

Abstract

The periosteum is a highly vascularised, collagen-rich tissue that plays a crucial role in directing bone repair. This is orchestrated primarily by its resident progenitor cell population. Indeed, preservation of periosteum integrity is critical for bone healing. Cells extracted from the periosteum retain their osteochondrogenic properties and as such are a promising basis for tissue engineering strategies for the repair of bone defects. However, the culture expansion conditions, and the way in which the cells are reintroduced to the defect site are critical aspects of successful translation. Indeed, expansion in human serum and implantation on biomimetic materials has previously been shown to improve *in vivo* bone formation. As such, this study aimed to develop a protocol to allow for the expansion of human periosteum derived cells (hPDCs) in a biomimetic periosteal-like environment. The expansion conditions were defined through the investigation of the bioactive cues involved in augmenting hPDC proliferative and multipotency characteristics, based on transcriptomic analysis of cells cultured in human serum. Master regulators of transcriptional networks were identified and an optimised periosteal derived-growth factor cocktail (PD-GFC; containing β-Estradiol, FGF2, TNFα, TGFβ, IGF-1 and PDGF-BB) was generated. Expansion of hPDCs in PD-GFC resulted in serum mimicry with regards to the cell morphology, proliferative capacity and chondrogenic differentiation. When incorporated into a 3D collagen-type-1 matrix and cultured in PD-GFC, the hPDCs migrated to the surface that represented the matrix topography of the periosteum cambium layer. Furthermore, gene expression analysis revealed a downregulated Wnt and TGFβ signature and an upregulation of CREB, which may indicate the hPDCs are recreating their progenitor cell signature. This study highlights the first stage in the development of a biomimetic periosteum which may have applications in bone repair.

Graphical Abstract
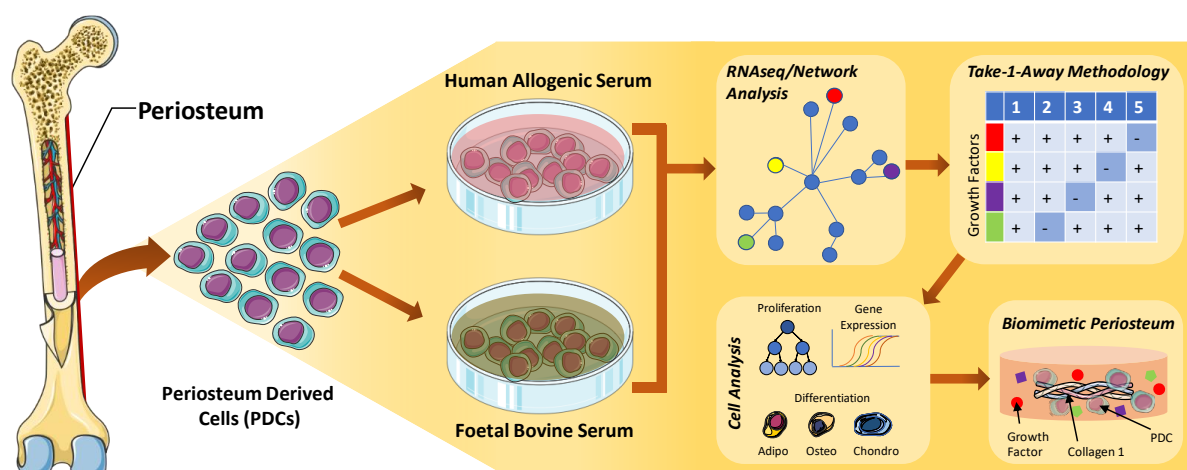
Schematic representation of the study "Mapping human serum induced gene networks as a basis for the creation of biomimetic periosteum for bone repair" (This figure was produced using Servier Medical Art).

Introduction

The periosteum is a highly vascularised connective tissue that covers bone. It is composed of two layers; an inner cambium layer that contains a skeletal stem cell population and an outer fibrous layer composed of fibroblasts embedded within a collagen type-1 matrix (1)(2)(3). Collagen fibres located in the periosteum are relatively small and compact compared to collagen bundles found in the skin (3). The periosteum stem cell population located in the cambium layer acts as a major participant in bone development and fracture healing (4)(5). This population of multipotent cells are capable of self-renewing and differentiating into osteogenic and chondrogenic lineages, which is partly dependent on the mechanical stabilisation of the fracture (4)(6). During endochondral ossification, for non-stabilised fracture repair, the periosteum contributes up to 90% of the chondrogenic cells required for the early cartilaginous callus (7).

Bone has an extraordinary capacity for repair, however, repair fails when the defect reaches a critical size and/or becomes a non-union (8). These bone defects are typically in compromised conditions such as tumours, infection, major trauma or congenital malformation resulting in significant disruption of the periosteum layer (9). Various surgical procedures have been implemented to overcome failed healing including the use of autologous bone, which is the current gold standard. Additionally, generation of pseudo-periosteum using the masquelet membrane technique and periosteum grafts have shown potential for bone repair (10). Despite surgical advances, there is an unmet medical need for an 'off the shelf' regenerative solution for large bone defects. This would overcome many of the caveats associated with surgery, including donor site morbidity, risk of infection and discomfort (4). To overcome these issues, regenerative medicine aims to repair damaged tissue using cell-based therapies.

Periosteum derived cells (PDCs) are a promising cell source for bone repair, predominantly due to their intrinsic bone forming capacity (11)(12). Indeed, this cell population displays multipotent characteristics at single cell level and the ability to form a bone ossicle with haematopoietic compartment *in vivo* (13)(14). However, cell potency is lost during expansion over long periods of time, hence currently there is a limited window to apply these cells to clinical strategies (15). This is similar to other adult stem cell populations and as such there has been a defined effort to enhance the proliferative and differentiation capacity through optimisation of culture conditions. Currently, human mesenchymal stromal cells (hMSCs) are generally expanded in conventional culture media using foetal bovine serum (FBS), which provides bioactive molecules such as growth factors, hormones and proteins necessary for cell growth and function (15). However, a myriad of disadvantages and limitations are associated with its use. Indeed, it is an ill-defined supplement and is inconsistent with regards to the quality and quantity of bioactive compounds present thus resulting in lot-to-lot variability (16)(17). Additionally, the use of a xenogenic serum could result in possible immune-mediated rejection if used

for clinical translation of cell therapies (18). Furthermore, ethical concerns associated with the harvesting of FBS from foetal calves presents another significant challenge to its use (19).

Various serum-free and xeno-free media have been developed in an attempt to negate the potential variability and safety concerns associated with the use of animal serum in clinical applications (20). Indeed, we have reported the beneficial effect of human allogeneic serum (hAS) on the *in vitro* differentiation and expansion of human PDCs (hPDCs). These findings were translated successfully *in vivo* where cells expanded in hAS outperformed FBS expanded cells in bone forming capacity, thus demonstrating culture memory from *in vitro* expansion (11). Interestingly, platelet lysate has also been shown to increase hPDC bone forming capacity (21). Nevertheless, the use of hAS for clinical applications would require extensive screening and a well-characterised pool of donors, which could prove problematic in a clinical setting. Therefore, it is attractive to develop alternative methods of incorporating the necessary factors required to maintain the proliferative and progenitor-like characteristics of hPDCs. Furthermore, an appropriate scaffold that replicates the periosteum and allows the creation of a suitable delivery device is required for clinical translation.

Herein a protocol for the expansion of hPDCs in a biomimetic periosteal-like environment to facilitate delivery to a bone defect is proposed. The expansion conditions were defined through the transcriptomic analysis of cells cultured in hAS. Gene network analysis was utilised for the identification of the key master regulators activated by hAS cultured conditions. Through the identification and careful selection of these growth factors, we were able to achieve serum mimicry with regards to cell morphology, proliferative capacity and chondrogenic differentiation. When cells were incorporated into a 3D collagen type-1 rich matrix, the periosteal-derived growth factor cocktail (PD-GFC) caused the hPDCs to migrate to the surface representing the matrix topography of the periosteum cambium layer. Furthermore, gene expression analysis revealed downregulated Wnt and TGFβ with upregulated CREB signalling, which may indicate the hPDCs are recreating their progenitor cell signature. The successful development of this cell-specific cocktail is the first step in developing a periosteum-like environment that mimics the biology of the periosteum.

Materials and Methods

Human periosteum-derived cell cultures

hPDCs were isolated from biopsies obtained from patients undergoing orthopaedic surgery as described elsewhere (14)(13). Human Medical Research (KU Leuven) approved all procedures, and the patient informed consent forms were obtained. Subsequently, hPDCs from a pool of six different donors (Age = 14.9 ± 2.1 years; Male:Female = 4:2) were expanded in growth medium (GM) consisting of high-glucose Dulbecco's Modified Eagle's Medium (DMEM, Invitrogen, Paisley, UK) supplemented with 10% batch-tested foetal bovine serum (FBS) and antibiotics-antimycotic solution (100 units/ml

penicillin, 100 µg/ml streptomycin and 0.25 µg/ml amphotericin B; Invitrogen, Paisley, UK) to passage 5. All experiments described herein were performed in pooled hPDCs at passage 6. We have previously published the CD marker profile (CD73+, CD90+ and CD105+), tri-linage differentiation capacity (osteogenic, chondrogenic, adipogenic) and *in vivo* bone forming capacity (bone ossicle with marrow) of this donor pooled population (13)(11).

Selection of growth factors by RNAseq

We have previously tested the three hAS serum pools (minimum of 15 donors) used herein, with two different hPDC cell pools and observed very similar growth characteristics with each combination. This data is reported in Roberts *et al* (2014). To analyse the effects of the culture systems on the hPDCs, RNA sequencing (RNAseq) was performed on the aforementioned hPDC pool at sub-confluence (initial seeding density 1000 cells/cm^2) following culture for 6 days in hAS serum (n=3; donor pooled) or FBS (n=3; different Gibco batch). RNA was extracted using the Illumina TruSeq Standard Total RNA Sample Prep Kit (Illumina, US). RNA integrity was validated using a BioAnalyzer (Agilent).

RNAseq was performed at the Nucleomics Core (KU Leuven; Belgium). Libraries were generated from 2 µg RNA using the TruSeq library prep kit (Illumina, San Diego) as per the manufacturer's recommendations. Sequencing of all samples was carried out on the HiSeq2000 (Illumina), with read lengths of 50 base pairs. Between 25-39.3 million reads were sequenced for each sample. Distributions of the average read quality was calculated using the ShortRead 1.18.0 package from Bioconductor (http://www.bioconductor.org). Base calling accuracy, measured by the Phred quality score, was measured in all samples, with values of ≥30.

Pre-processed reads were aligned with the reference genome of Homo sapiens (GRCh37.73) using Tophat v2.0.8b. Quality filtering to remove reads from the alignment that were non-primary mappings or had a mapping quality ≤ 20 was performed with SAMtools 0.1.19. The number of mapped reads varied between 17.7 and 28.3 million reads per sample. Subsequently, Cufflinks v2.1.1 was used to extract unique transcript-related features. A list of gene level coordinates was constructed by merging the exon chains of transcripts that belong to the same gene using mergeBed from the Bedtools v2.17.0 toolkit. The number of exons and number of transcripts was subsequently computed for each gene. Genes where reads could be attributed to more than one gene (ambiguous) or could not be attributed to any gene (no feature) or which all samples have less than 1 counts-per-million (absent) were removed. This left 15,518 identified genes. GC-content was corrected in each sample using full quantile normalization on bins of GC-content with the EDASeq package from Bioconductor. Between-sample normalization (sample-specific variation due to the library size and RNA composition) were corrected for using full quantile normalization with the EDASeq package from Bioconductor. A Relative Log Expression plot using log$_2$-scale normalized counts for each gene as expression level was constructed and resultant values of close to 0 indicated the normalization was successful. For each gene, the

expression levels of both conditions were estimated from the raw counts with the DESeq 1.14.0 package of Bioconductor and tested for differential expression based on a model using the negative binomial distribution. To select genes the corrected p-value was set at < 0.05 which resulted in 1331 differentially regulated genes ($\log_2$ ratio ≤ -1 or $\log_2$ ratio ≥ 1).

The dataset was validated using quantitative Polymerase Chain Reaction (qPCR; described below). Differentially regulated genes were selected based on fold change ratios from the RNAseq datasets between cells cultured in hAS compared to FBS. The genes selected for data validation demonstrated a high up/down regulated expression (fold change >20), moderate change (fold change 10-20) and minimal up/down regulation (fold change <10) (gene panel detailed in supplementary Figure 1). The genes that were significantly differentially expressed between hAS and FBS were initially interrogated through the online platform DAVID (Database for Annotation, Visualization and integrated Discovery, http://david.abcc.nciforf.gov/) to determine the prominent biological processes involved in each of these culture conditions. The data was further analysed using Ingenuity® Pathway Analysis (IPA®) (Qiagen, Netherlands) to identify activated networks and up-stream regulators controlling the divergent biology observed between hAS and FBS. All genes demonstrating a fold change >2 with respect to expression in hAS compared to FBS with a p-value <0.05 were extracted from the RNAseq data for analysis with IPA. Associated genomic relationships were generated including regulators indirectly connected to the primary targets observed, to help identify the upstream regulators. Factors were selected according to their relationships with ten gene networks. Factors identified as significant upstream regulators were mapped onto the gene networks to interrogate their function in respect to each of the identified processes. A literature search was performed to determine any precedent for each factor in mesenchymal cell expansion/culture and to select appropriate concentrations for further investigation.

Leave-one-factor-out strategy

Upstream regulators identified via IPA were assessed *in vitro* for their potential role in controlling hPDC gene expression, proliferation and metabolic activity. The selected factors (Vascular Endothelial Growth Factor α (VEGFα; 10 ng/mL, Peprotech, UK), Dexamethasone (1×10^{-8} M, Sigma), Wnt3A (10 ng/mL, R&D Systems), 17-β Estradiol (1×10^{-9} M, Sigma), Fibroblast growth factor-2 (FGF2; 10 ng/mL, ThermoFisher), Tumour Necrosis Factor α (TNFα; 5 ng/mL, Peprotech), Transforming Growth Factor (TGFβ; 10 ng/mL, Peprotech), Insulin Growth Factor-1 (IGF-1; 20 ng/mL, Peprotech) and Platelet Derived Growth Factor (PDGF-BB; 10 ng/mL, Peprotech) were applied in a 'leave-one-factor-out' strategy to identify the key regulators involved in stimulating the cells' proliferation and differentiation *in vitro*. hPDCs were seeded on a 24 well plate at a density of 1000 cells/cm^2 and cultured for seven days in the varying factor conditions supplemented with 1% FBS (concentration that when in combination with additional defined serum-free replacements the culture becomes notably defined;

(22)) in phenol red free, high glucose DMEM (Invitrogen through ThermoFisher Scientific, UK). Factors critical to analysed cell responses were combined to create PD-GFC.

Analysis of in vitro cell response

To assess metabolic changes the cells were also treated with PrestoBlue® Cell Viability Reagent (Thermo Fisher Scientific) following manufacturer's instructions. This Resazurin-based assay induces changes in absorbance at 600 nm which were recorded using a Tecan Infinite® 200 PRO plate reader. Double-stranded DNA (dsDNA) quantification was carried out using the Qubit® dsDNA High Sensitivity Assay Kit (Thermo Fisher Scientific) following manufacturer's instructions. Briefly, cell monolayers were lysed in RLT buffer (Qiagen) plus 10 μl/ml β-mercaptoethanol (Sigma Aldrich) (23). The lysate was diluted 1/10 in nuclease-free water (Sigma Aldrich). Readings were obtained using the Qubit™ 3.0 fluorometer and were calculated as total dsDNA [ng/μl]. Cell spreading was analysed by culturing cells for seven days at a cell density of 1000 cells/cm^2, which were subsequently fixed with 10% neutral buffered formalin (NBF) (Sigma, UK). Actin cytoskeleton was visualised through staining with phalloidin and nuclei counterstained with DAPI. Cell spreading was calculated via a Width: Length ratio measured digitally using ImageJ (National Institute of Health).

Quantitative PCR

Total RNA was isolated using the RNeasy kit (Qiagen, Germany) following manufacturer's instructions. RNA was quantified using a NanoDrop spectrophotometer measuring at 260/280 nm, and 1 μg RNA/sample was reverse transcribed using the High Capacity cDNA Reverse Transcriptase Kit (Thermo Fisher Scientific, Paisley, UK) with the program: 25°C for 10 min, 37°C for 120 min, 85°C for 5 min, and infinite hold at 4°C. Transcribed cDNA was assessed via the CFX96 Touch™ Real-Time PCR Detection System (40 cycles) using the iTaq Universal SYBR Green Supermix (Bio-Rad, Hertfordshire, UK). Primers were designed using Primer3 (listed in supplementary Table 1) and were designed to span an intron to isolate RNA specific amplification. Relative differences in expression were calculated using $2^{-\Delta\Delta Ct}$ (24) normalised to HPRT expression.

Analysis of hPDC growth kinetics

The effect of PD-GFC on hPDC characteristics was assessed by expanding the cells in either PD-GFC medium or conventional GM. Cells were initially grown in conventional GM containing 10% or 1% FBS until confluency was reached and further subcultured in either GM (containing either 1% FBS or 10% FBS) or PD-GFC medium over 4 passages (n= 3). Cumulative population doubling was calculated using the following equation: PDL = 3.32 (log Xe – log Xb) + S; where Xb is the cell number at the beginning of the culture, Xe is the cell number at the end of the culture and S is the population doublings at the start of the culture.

Analysis of hPDC differentiation

Previously expanded cells (in either 10% FBS or PD-GFC) were subcultured at 70% confluency and then assessed for their differentiation capacity. Osteogenic differentiation was assessed using a defined osteogenic growth factor cocktail (25) on hPDCs passaged twice in either GM or PD-GFC- seeded at a density of 3000 cells/cm^2 in their initial growth mediums for 24hrs. The media was replaced with conventional growth medium supplemented with Ascorbate-2-phosphate (57 µM, Sigma), TGF-β1 (10 ng/mL, Peprotech), Epidermal Growth Factor (EGF; 20 ng/mL, Invitrogen), Interleukin-6 (IL-6; 10 ng/mL, Peprotech), Calcium ions (3 mM) and Phosphate ions (2 mM). The cells were differentiated for a period of 7 days with media changed every 48 hrs. Differentiation was assessed through staining with alizarin red solution (pH 4.2). Quantification of calcium mineral deposits was performed by dissolving the incorporated dye with 10% cetylpyridinium chloride (in deionised water) for 60 minutes at room temperature. Absorbance was measured spectrophotometrically at 570 nm.

Chondrogenic differentiation was assessed on hPDCs expanded over 3 passages in either GM or PD-GFC and further seeded in high-density micromasses at a cell density of 5,000 cells/µL. Cells were allowed to adhere before culturing in chondrogenic medium consisting of low glucose DMEM (Invitrogen), 1x Insulin-transferrin-selenium supplement (Corning, UK), Dexamethasone (100 nM, Sigma), Y27632 (10 µM, Axon, UK), ascorbic acid (50 µg/mL, Sigma), proline (40 µg/mL, Sigma) and TGF-β1 (10 ng/mL, Peprotech) for 7 days. Differentiation was evaluated by staining with Alcian Blue (Sigma) (pH 2.0) overnight at room temperature. Quantification of proteoglycans was carried out by extracting the Alcian blue dye from the micromass using 6M guanidine hydrochloride and measuring the absorbance at 620 nm.

Adipogenic differentiation was assessed following hPDC culture over two passages in either GM or PD-GFC at a cell density of 30,000 cells/well in a 48 well plate for a period of 21 days. The cells were seeded in growth medium until the cells reached confluency after 48hrs. Once confluency was reached the media was substituted with adipogenic differentiation media containing 10% FBS, Insulin (1 µg/mL, Sigma), Dexamethasone (0.1 µM, Sigma), Isobutylmethylxanthine (IBMX; 4.5 µM, Sigma) and indomethacin (125 µM, Sigma). Media was changed every 2 days. Production of fat droplets was assessed using oil red O stain and lipid droplet area quantified using ImageJ (National Institute of Health). Gene expression analysis was performed on stem, osteogenic, chondrogenic and adipogenic markers and qPCR conducted as previously described.

Formation of collagen-type 1-hPDC seeded scaffold

hPDCs were expanded until 80% confluency was reached. Rat tail collagen type-1 (First Link, UK) gels were prepared according to the RAFT protocol. A collagen master-mix was prepared containing 10% 10x DMEM, 80% Rat tail collagen type-1 (2.05 mg/ml in 0.6% acetic acid) and a 10% neutralising agent composed of 10 M NaOH and Hepes buffer (ThermoFisher Scientific, UK) (26). The collagen

solution was set on ice for a minimum of 30 minutes to allow for the movement of air bubbles out of the solution. The cells were prepared and incorporated into the collagen master mix to produce collagen scaffolds with a density of 100,000 cells per gel. A volume of 1.3 mL of the collagen master mix was dispensed into 24 well plates. The gels were allowed to gelate at 37℃ for 15 minutes allowing for fibrillogenesis of the collagen hydrogel, comprised of a network of intertwined fibrils with no inherent orientation consisting of a large excess fluid to collagen ratio (27). To achieve a denser (10%) collagen matrix, the gelated constructs underwent plastic compression using a hydrophilic RAFT absorber, following the Lonza 'RAFT 3D Cell Culture' protocol. Briefly, the absorber was placed on top of the gel for 15 minutes to expel the fluid content through the main (basal) fluid leaving surface of the gel. This resulted in a ~50 fold increase in collagen density (28). Following plastic compression, the absorber was removed and 1 mL of GM was added to the well. After 24hrs, the media was substituted with either 10% FBS containing medium or the PD-GFC and cultures were allowed to incubate for a period of 14 days. The collagen gels were subjected to histological analysis: paraffin embedded sections were stained for cell cytoplasm and nuclei with haematoxylin and eosin, respectively.

RT² Profiler PCR Array of Human stem cell signalling

To further interrogate the signalling mechanisms involved when the hPDCs were cultured in either FBS or PD-GFC in 3D, an RT² Profiler PCR array (Qiagen) specific for stem cell-associated signalling pathways was utilised. The array profiles 84 key genes representative of six different signal transduction pathways associated with identification, growth and differentiation of stem cells. The hPDCs were embedded within the collagen type-1 matrix as detailed above and subsequently cultured in either FBS containing growth media or PD-GFC for a period of 14 days. Samples were lysed using TRI reagent and RNA isolated using the chloroform phase separation technique and subsequently processed using the RNeasy Kit (Qiagen) according to manufacturer's instructions (29). Single strand cDNA was transcribed using 1 µg total RNA, synthesised using the RT² first strand kit (Qiagen). Real-time PCR was performed using the RT² profiler array system according to manufacturer's instructions in combination with RT² SYBR® Green qPCR Mastermix (Qiagen) in a Biorad CFX96 PCR system (Biorad). Data Analysis was conducted using a web-based RT² PCR Profiler PCR array data analysis software (Qiagen). Genes were identified as up or downregulated with a fold change cut off of 2, with a corresponding p-value <0.05. P-values calculated based on student's t-test of the replicate $2^{-\Delta\Delta Ct}$ values for each gene in the FBS group and corresponding PD-GFC experimental group.

Stiffness of native periosteum and collagen-type 1 scaffold

Native bovine periosteum and seeded 10% collagen type-1 cell laden scaffolds (following 14 days culture in PD-GFC; n=3) were washed with PBS and embedded in optimal cutting temperature compound (OCT). Embedded samples were cryosectioned into 10 µm sections, transferred onto glass

slides and stored at room temperature. Atomic Force Microscopy (AFM) was performed on these samples using a JPK Nanowizard 1 AFM (JPK Instruments Ltd, Germany) with RFESPA-75 cantilever (k=0.3N/m). 100 measurements were performed within a 10 μm^2 surface area in 6 locations of each tested region within the tissue/scaffold.

Statistical Analysis

Data are expressed as mean ± standard error of the mean (SEM). Statistical significance was determined using one-way ANOVA with Fisher's LSD post hoc corrections applied or student's t-test. Statistical significance is indicated on all graphs as follows: *p<0.05, **p<0.01, ***p<0.001 (n=3). All statistical analysis was performed using GraphPad Prism version 6.0f for windows (GraphPad Prism Software, La Jolla California USA, www.graphpad.com).

Results

Identifying the regulators associated with hAS induced hPDC potency

hPDCs cultured in 10% FBS and 10% hAS for 6 days were subjected to RNASeq to analyse the transcriptomic profile of the cells in each condition. Prior to conducting further analysis with the data, the RNA Seq dataset was validated by qPCR profiling of the following markers: Human Transgelin 3 (TAGLN3), BCL2 related protein A1 (BCL2A1), Sulfotransferase family 1B member 1 (SULT1B1), C-X-C motif chemokine ligand 22 (CXCL2), PDK1 family protein kinase (PDKA4), Matrix metallopeptidase 1 (MMP1), Semaphorin 3A (SEMA3A), Angiopoietin-like 1 (ANGPTL1), Platelet derived growth factor subunit A (PDGFA), Noggin (NOG), Alpha kinase 2 (ALPK2), Cartilage intermediate layer protein 2 (CILP2), Insulin like growth factor 1(IGF-1), and Fibroblast growth factor 9 (FGF9). Relative expression values obtained using qPCR were comparable to those measured by RNA Seq with no significant differences observed (Supplementary Figure 1).

To determine the specific factors involved in regulating the cell's characteristics when cultured in hAS relative to FBS, IPA software generated a list of all upstream regulators (factors that are predicted to have a downstream effect on other molecules) associated with multiple targets within each identified pathway (Supplementary Table 2). The upstream regulators were arranged with respect to their overlap p-value (Right tail Fisher's exact test) which measures whether a statistically significant overlap is present between the experimental data set and the genes regulated by the upstream transcriptional regulators. The regulators with a significant overlap are predicted to have a significant effect within the culture system. The top 20 upstream regulators were then recorded as potential factors responsible for the characteristics observed in cells cultured in hAS.

An additional methodology incorporated in the identification of key factors was the assessment of gene networks (Supplementary Table 3), whereby hub genes with direct and indirect gene/protein interactions were identified. To validate the top 20 upstream regulators, each was mapped to the network, and genes that identified as both upstream regulators and hub genes within these networks were recorded. Two networks associated with embryonic, organismal, tissue development and cellular movement, haematological system development and function, immune cell trafficking were identified with the most recorded differential genes (Figure 1).

To further assess the validity of the selected factors a literature search was carried out on each to identify any known involvement in inducing cellular proliferation, bone formation or stemness (Supplementary Table 4). This resulted in 9 factors being selected for further analysis, including VEGF, Dexamethasone, Wnt3A, β-Estradiol, FGF2, TNFα, TGFβ, IGF-1 and PDGF-BB.
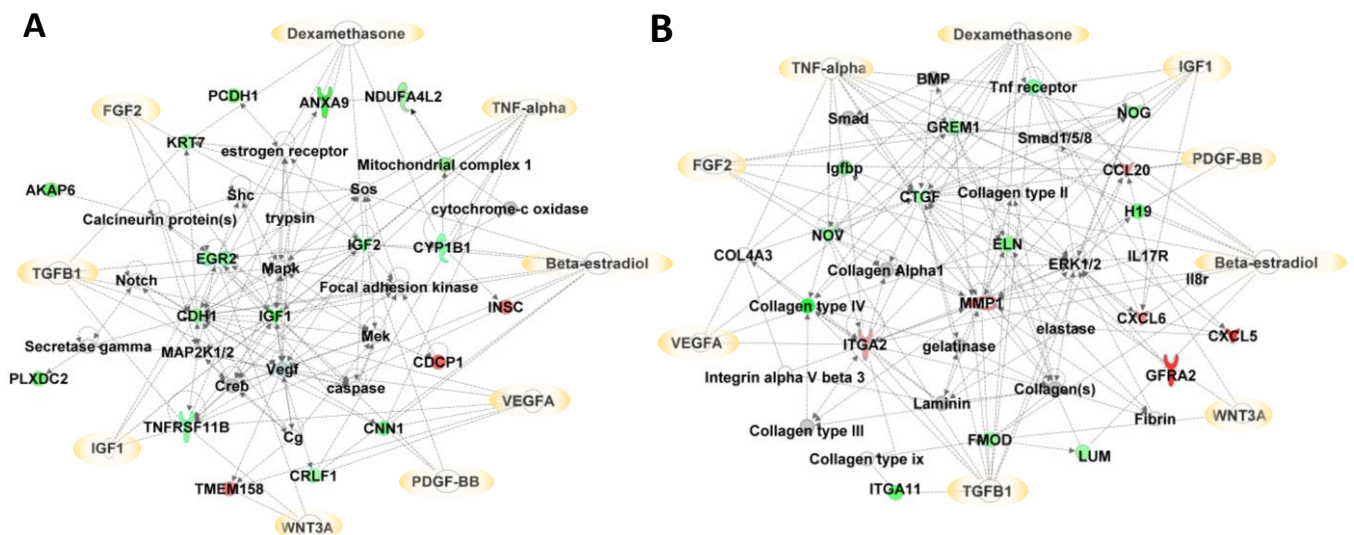

Figure 1: Gene networks associated with hAS culture of hPDCs A) Predicted upstream regulators integrated within a network involving Embryonic Development, Organismal Development, and Tissue Development. **B)** Predicted upstream regulators integrated within a network involving Cellular Movement, Hematological System Development and Function, and Immune Cell Trafficking. Upstream regulators selected for the PD-GFC are represented on both networks. Red indicates up-regulation whilst green indicates down-regulation. Grey indicates genes that are significantly changed in expression by less than 2-fold and white represents genes not significantly altered in the study but have been incorporated into the network through relationships with other molecules. Yellow indicates potential upstream regulators. Networks created in Ingenuity Pathway Analysis (IPA; Qiagen).

Assessing the effects of the selected factors on hPDC culture dynamics

The effect of each selected factor on hPDC biology was assessed using a "leave-one-factor-out" strategy, which was aimed at identifying the factors that induce cellular proliferation and a gene expression profile with enhanced stem and osteochondrogenic gene expression (Figure 2). hPDCs were cultured in the various conditions for a period of 7 days. The condition containing all factors was used

as a reference to evaluate the impact of each individual factor on proliferation and cellular metabolism (Figure 2B), and the expression of stem (Nestin (30) and Prx1 (31) based on previously published data indicating their relevance in the identification of cells from mesenchymal origin with apparent plasticity), early osteogenic and chondrogenic gene markers (Figure 2A). A positive regulation upon elimination of a factor compared to the reference indicated that this factor had a negative effect on the measurement. In this regard, we identified FGF2 as a strong inducer of proliferation (2.2 fold decrease in DNA content upon its elimination, $p<0.001$), metabolism (1.25 fold decrease in metabolic activity) and stemness (*NESTIN:* 1.2 fold decrease; *PRX1*: 1.7 fold decrease, $p<0.05$), however, minimal effects were observed with regards to early osteogenic (*RUNX2:* 1.4 fold increase*, ALP: 1.2 fold increase*) and chondrogenic (*SOX9:* 1.2 fold decrease and *COL2A1:* 2.2 fold increase, $p<0.001$) markers. TGFβ on the other hand had a minimal effect when considering metabolism (1.1-fold increase, $p<0.05$), however its removal decreased the expression of *NESTIN* (1.9-fold decrease, $p<0.01$), *RUNX2* (2.5-fold decrease, $p<0.01$), *ALP* (6-fold decrease, $p<0.001$) and *COL2A1* (10-fold decrease, $p<0.05$).

TNFα and βEstradiol were the only molecules that when removed induced a significant increase in the committed osteoblast marker ALP. As the primary goal of this study was to define culture conditions that allow the expansion of hPDCs in the absence of differentiation, both were retained in the culture conditions. In the case of IGF-1 and PDGF-BB, their removal caused minimal change in any tested parameter, however, removal caused the appearance of a heterogeneous culture and/or stress fibres within the cells and as such both were retained (Supplementary Figure 2).

Eliminating dexamethasone resulted in a significant increase of all tested gene markers (*NESTIN*: 1.8-fold, $p<0.001$; *PRX1*: 1.4-fold, $p<0.001$; *RUNX2*: 1.5-fold, $p<0.001$; *SOX9*: 1.86-fold, $p<0.001$; *COL2A1*: 0.8-fold, $p<0.01$) with the exception of *ALP* (5-fold decrease, $p<0.001$). With this reasoning, dexamethasone was eliminated from the growth factor cocktail. Additionally, eliminating WNT3A from the study significantly increased cellular proliferation (0.3-fold increase, $p<0.05$) with no significant effect on cellular metabolism and all tested gene markers and was thus eliminated from the study. Lastly, eliminating VEGF caused a significant increase in proliferation (0.4-fold change, $p<0.01$) and cellular metabolism (0.4-fold change, $p<0.01$), with no significant effect on tested gene markers, and was thus eliminated from the study.

Using this methodology, a refined cocktail of factors was generated that included βEstradiol, FGF2, TNFα, TGFβ, IGF-1 and PDGF-BB. This was termed periosteum-derived growth factor cocktail (PD-GFC). The morphology of cells cultured in hAS and PD-GFC was similar (Figure 2C) indicating potential equivalence of the culture conditions based on cell phenotype.
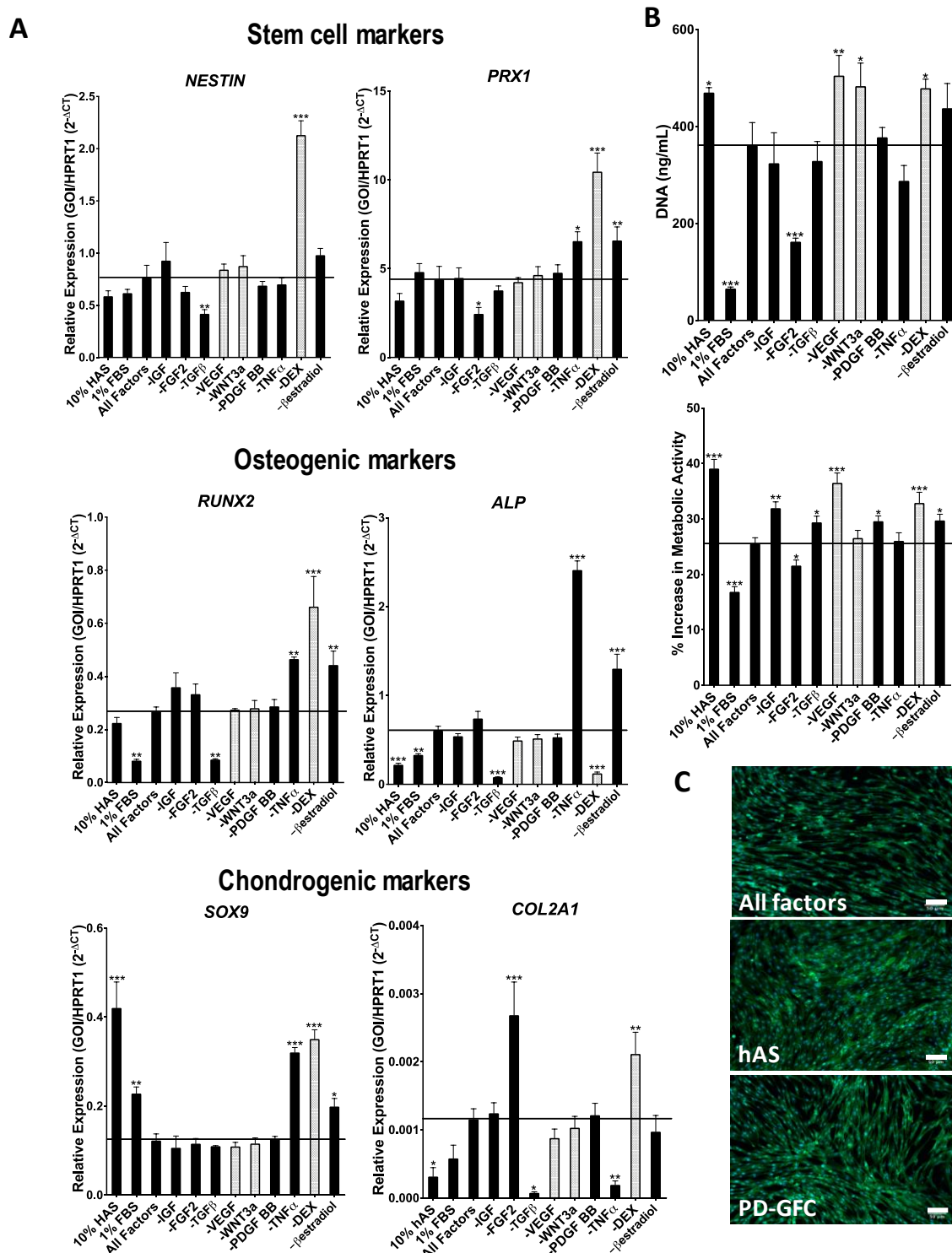
Figure 2: Leave-one-factor-out strategy to identify factors important for hPDC potency A) Expression of stem markers; *NESTIN* and *PRX1*, osteogenic markers; *RUNX2* and *ALP*, and chondrogenic markers; *COL2A1* and *SOX9*. Horizontal line indicates expression levels relative to the 'all factors' condition. **B)** Quantification of cellular DNA to assess proliferation and percentage increase in metabolic activity was assessed. Growth factors eliminated from the study are represented as grey bars. (Data are presented as the mean ±S.E.M, Statistical analysis performed using one-way ANOVA, uncorrected Fischer's LSD; ***$p < 0.001$; **$p < 0.01$; *$p < 0.05$; n=3). **C)** Representative fluorescence images illustrating nuclear DAPI staining and cytoskeleton staining of hPDCs cultured in All factors, hAS, and the refined PD-GFC. Note the similar morphology of hPDCs cultured in PD-GFC and hAS (scale bar 50μm).

hPDCs cultured in PD-GFC display differences in cellular morphology and lineage commitment in vitro compared to 10% FBS

To assess the efficacy of the PD-GFC for hPDC expansion, hPDCs were treated with the PD-GFC over multiple passages to observe its effect on the cell's proliferation rate relative to 10% and 1% FBS. Culture of hPDCs in PD-GFC resulted in a significantly higher cumulative population doublings over time and per passage (after P8) compared to 10% FBS and 1% FBS ($P < 0.05$) (Figure 3A and B). The cells remained proliferative after P10 and appeared morphologically normal. Data associated with a typical passage in each of the media formulations is shown in Supplementary Table 5. However, it cannot be categorically stated from these data that no senescent cells were present within the cultures. With regards to cell spreading, the ratio of the cells width to length was quantified when treated with 1% FBS, 10%FBS and PD-GFC (Figure 3B). hPDCs cultured in PD-GFC resulted in a 3.1-fold lower ratio than when cultured in 10% FBS ($p < 0.001$; Figure 3C), which follows the same trend as previously published for hAS-cultured cells (11). Furthermore, the expression of mesenchymal stem marker *NESTIN* was higher at each passage when cultured in PD-GFC compared to 10% FBS (1.9, $p < 0.01$; 3.3, $p < 0.001$; 2.0, $p < 0.01$; and 2.6-fold, $p < 0.001$ higher at passage 7-10 respectively). In cells treated with the PD-GFC relative to 10% FBS, *PRX1* displayed an increase in expression in PD-GFC treated cells at passage 7 (1.3- fold, ns), 8 (1.3-fold $p < 0.05$), 9 (1.2-fold, ns) and passage 10 (2.0, $p < 0.001$) when compared to 10% FBS (Figure 3D). The expression of the osteogenic transcription factor *RUNX2* was increased in the PD-GFC treated cells, with a significant increase observed at passages 8 (3.4-fold, $p < 0.001$), 9 (1.8-fold, $p < 0.05$) and 10 (5.0-fold, $p < 0.001$). Interestingly, *ALP* expression was lower in PD-GFC treated cells and significantly lower at P8 (3.0-fold, $p < 0.01$) and 10 (1.5- fold, $p < 0.01$). With regards to chondrogenic markers, *SOX9* displayed a lower expression profile at passages 7-10 in cells treated with PD-GFC though not significant. *COL2A1* expression was however, significantly up regulated in PD-GFC treated cells at passage 7-10 (17.0 ($p < 0.01$), 11.4 ($p < 0.001$), 4.8 ($p < 0.05$), 5.0 ($p < 0.01$)- fold, respectively) relative to 10% FBS.
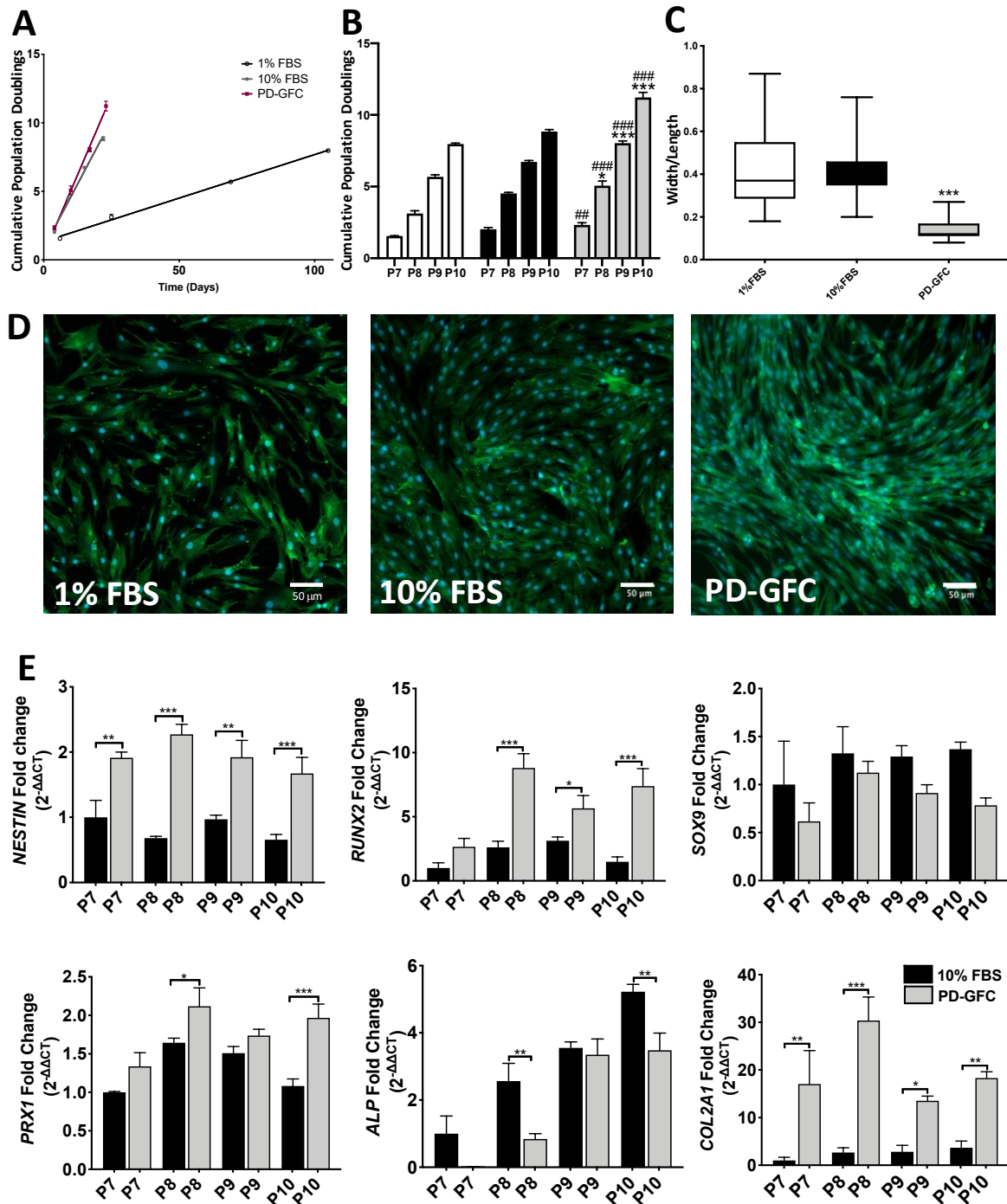
Figure 3: Validation of PD-GFC as a defined media for hPDC culture. A) Population growth curves of hPDCs expanded in 1% FBS, 10%FBS and PD-GFC. **B)** Cumulative population doublings in all three media conditions at all tested passages 7-10 (P7-10). Significant differences observed in cells expanded in PD-GFC relative to FBS (*, PD-GFC relative to 10% FBS; #, PD-GFC relative to 1% FBS). **C)** Cell spreading of hPDCs in 1%FBS, 10%FBS and PD-GFC. Data are presented as the mean ±S.E.M. Statistical analysis performed using one-way ANOVA, uncorrected Fischer's LSD; T-test, Mann-Whitney test (***,###$p<0.001$; **,##$p<0.01$; *$p<0.05$; n=3). **D)** Representative fluorescence images illustrating cellular spreading of hPDCs cultured in 1% FBS, 10%FBS and PD-GFC for a period of 6 days (nuclear DAPI staining and cytoskeleton staining with Phalloidin; Scale= 50 m). **E)** Stem markers; *NESTIN* and *PRX1*, osteogenic markers; *RUNX2* and *ALP*, and chondrogenic markers; *COL2A1* and *SOX9*; expression measured using qPCR. (Data are presented as mean ±S.E.M, Statistical analysis performed using one-way ANOVA, uncorrected Fischer's LSD; ***$p<0.001$; **$p<0.01$; *$p<0.05$; n=3)

15

Expansion in PD-GFC maintains hPDC osteochondrogenic potential

Following expansion of hPDCs through multiple passages (as mentioned above), a subset of cells were subjected to standard chondrogenic, osteogenic and adipogenic differentiation conditions. The data illustrated in Figure 4A is a representation of the chondrogenic differentiation assay. The micromass cultures treated with standard chondrogenic factors resulted in a 1.8-fold increase ($p<0.05$) in alcian blue stain, indicative of proteoglycan deposition in cells previously expanded in the PD-GFC relative to 10% FBS (Figure 4A). The early chondrogenic transcription factor *SOX9* was significantly up regulated (2.3-fold, $p<0.001$) in the PD-GFC primed cells compared to 10% FBS cultured cells.

Osteogenic differentiation was conducted for 7 days (Figure 4B), with no significant differences in calcium phosphate deposition illustrated by an alizarin red stain between the two expansion medias. A modest reduction in the expression of the osteogenic transcription factor *RUNX2* (1.3-fold, $p<0.01$) was observed in PD-GFC cultured cells compared to 10% FBS.

The cells were further subjected to an adipogenic differentiation assay for 21 days (Figure 4C). An oil red O stain was performed identifying the formation of fat droplets. Cells cultured in 10% FBS prior to the differentiation assay resulted in the formation of large fat droplets. However, cells cultured in PD-GFC resulted in immature fat droplet formation after the 21-day period, further confirmed by a 23.4-fold decrease in lipid droplets (Figure 4C). A 52.6-fold decrease in the adipogenic marker FABP4 was observed in PD-GFC expanded cells relative to 10% FBS.
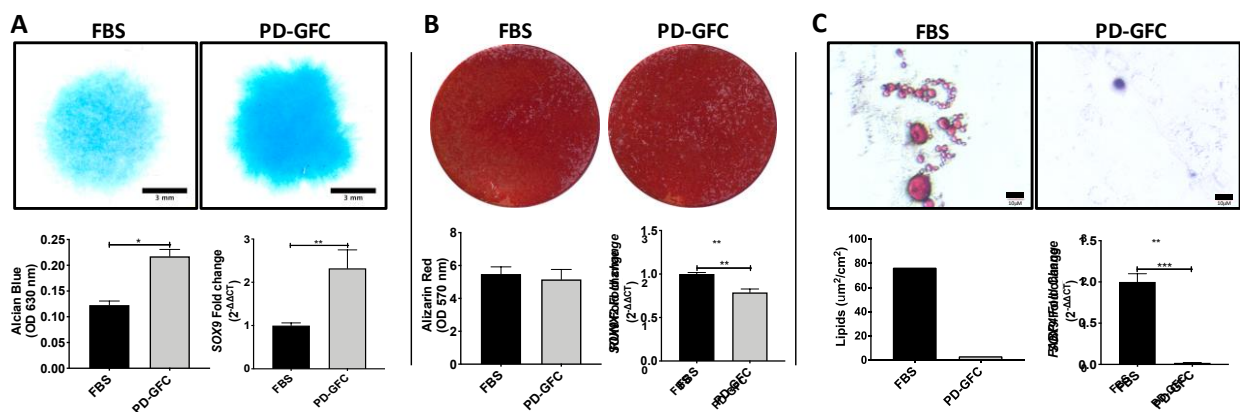

Figure 4: Defining the effect of PD-GFC on hPDC differentiation and potency A) Chondrogenic differentiation was conducted after hPDCs underwent 4 passages in either 10% FBS or PD-GFC. Micromasses were stained and quantified with Alcian blue at day 7, with *SOX9* transcription factor analysed by qPCR (Scale bar =3 mm). hPDCs cultured in PD-GFC had a significantly higher glycosaminoglycan content compared to hPDCs cultured in 10% FBS and significant increases in *SOX9* expression ($p<0.01$). **B)** After 2 passages, an osteogenic differentiation assay was conducted for 7 days, with no significant differences in calcium phosphate deposition illustrated by alizarin red stain, however, a significantly lower expression of osteogenic related transcription factors *RUNX2* in PD-GFC cultured cells. **C)** After 2 passages, an adipogenic differentiation assay was performed and fat droplets analysed using Oil red O stain. Distinct fat droplets observed in cells cultured in 10% FBS with immature fat

droplets observed in PD-GFC cultured cells, with a lower gene expression of the adipogenic associated maker *FABP4* compared to 10% FBS cultured cells. (Data are presented as the mean ± S.E.M, Statistical analysis performed using one-way ANOVA, uncorrected Fischer's LSD; ***p<0.001; **p<0.01; *p<0.05; n=3, scale bar= 10 μm).

hPDCs encapsulated within a 3D Collagen type-1 matrix and cultured in PD-GFC display periosteum like characteristics

hPDCs were embedded within a 3D collagen type-1 matrix. The aim of this study was to further recapitulate the *in vivo* periosteum microenvironment by incorporating the cell populations in optimised culture conditions in a relevant matrix. 100,000 cells were either seeded in a 2D monolayer or embedded within 10% (plastic compressed) 3D collagen type-1 matrix. After a 14-day culture, the constructs were paraffin embedded, sectioned and stained with haematoxylin and eosin to observe the collagen and cell distribution. Upon plastic compression of the collagen gels, a dense layer of collagen was visible on the fluid leaving surface (FLS) compared to the rest of scaffold (Figure 5B). The 10% FBS cultured constructs had cells dispersed throughout the matrix. However, when cultured in PD-GFC, more hPDCs were visible within the construct with the majority of cells aligned along the FLS of the scaffold. Interestingly, this did not occur when using a lower cell density of 30,000 cells (Supplementary Figure 3A). Intriguingly, the organisation of the cells mirrored that of native periosteum (Figure 5A). Furthermore, when comparing the gene expression profile of this biomimetic construct to cells cultured in standard conditions, an upregulation of genes associated with periosteal biology was observed with the exception of Prx1 (Supplementary Figure 3B). We hypothesised that this cell organisation was due to the biophysical properties of this region, and as such set out to analyse the morphology of the collagen fibrils and the matrix stiffness of both the native periosteum and hPDC laden collagen type 1 scaffold following 14 days culture in PD-GFC. As seen in Figure 5E, Atomic Force Microscopy (AFM) stiffness measurements of either side of the scaffold revealed no difference, unlike native periosteum where the fibrous layer was 1.47-fold stiffer than the cambium layer. Interestingly, the scaffold stiffness was in the same range as that observed with periosteum (Scaffold = 5.40-5.45 GPa, Periosteum = 4.55-6.69 GPa). With regards to collagen fibril morphology, collagen fibril structure and orientation was similar between the FLS and cambium layer, respectively. A similar fibril morphology was also observed between the bottom of the scaffold and the fibrous layer of the periosteum (Figure 5C).
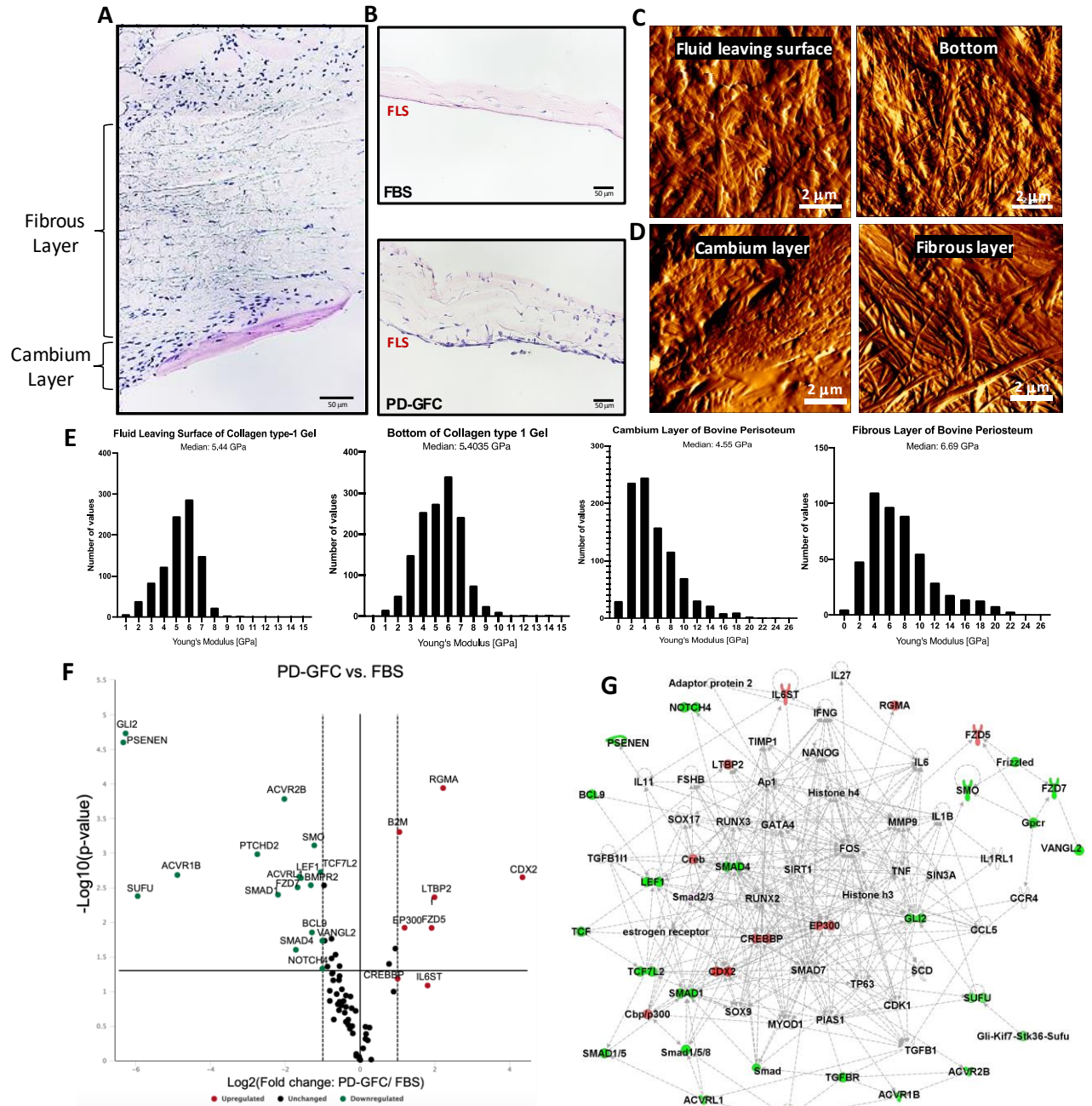
Figure 5: Effect of PD-GFC on hPDCs cultured in a collagen matrix – creation of an engineered periosteum. hPDCs were cultured in either a 2D monolayer or a 3D environment containing 10% rat-tail collagen type 1 for a period of 7 and 14 days. The cells were exposed to either 10% FBS or PD-GFC in all aforementioned environments. **A)** H&E stain of bovine periosteum illustrating the cell dense-cambium layer and fibrous layer (scale bar: 50 μm). **B)** Collagen scaffolds cultured in either 10% FBS or PD-GFC at day 14. Cellular migration of hPDC visible towards the dense fluid leaving surface (FLS) in PD-GFC cultured scaffolds (scale bar: 50 μm). **C)** Images of collagen fibrils in PD-GFC cultured collagen type 1 scaffolds at the FLS and bottom surface of the scaffold (scale bar: 2μm). **D)** Images of collagen fibril orientation of a native periosteum within the cambium layer and fibrous region of the tissue. **E)** Stiffness measurements of native periosteum tissue and collagen type 1 scaffold. The graphs illustrate the median stiffness from each specific region. **F)** Volcano plot of genes significantly up and down regulated in PD-GFC cultured hPDCs in a 3D construct relative to FBS cultured cells (p<0.05) with a fold change >2. **G)** Gene network representing various signalling interactions between genes that were significantly up and down regulated in FBS vs. PD-FC cultured constructs (created in IPA).

Identification of signal transduction factors associated with PD-GFC cultured hPDCs

To further determine the underlying mechanisms involved in PD-GFC culturing of hPDCs in a 3D environment, cells were embedded in a 3D collagen type 1 matrix and cultured in either 10% FBS or PD-GFC for 14 days. RNA was extracted and changes in gene expression was observed using the human stem cell signalling array. Of the 84 genes examined, 9 genes were significantly upregulated in PD-GFC cultured cells relative to FBS and 17 genes were significantly downregulated in PD-GFC cultured cells relative to FBS with a 2-fold or more change in expression, illustrated in the volcano plot (Figure 5F). The data was further interrogated using IPA to define the likely gene network associated with the transcriptional profile. The gene network shown in Figure 5G represents genes from the PCR array that were either up (red) or downregulated (green) with additional genes that are likely to play a role also represented. It was noted that TGF superfamily (ACVR2B, ACVR1B, SMAD1 and SMAD4), Wnt signalling (FZD7, TCF and LEF1) and Hedgehog (GLI2, PTCHD2) were downregulated with an upregulation of CREB associated pathways (CREBBP and EP300).

Discussion

The identification of gene networks that are activated during stem cell expansion, whilst retaining potency, is an essential step in tissue engineering and regenerative medicine. Although generic defined culture conditions have been commercialised, many of these contain a proprietary formulation of growth factors and small molecules and as such delineating data generated using these media remains difficult. We have previously demonstrated the superiority of hAS over FBS in supporting hPDC expansion, osteochondral differentiation and *in vivo* bone tissue formation (11). However, the specific signals involved in this effect are largely unknown. Through the comparison of gene expression in hPDCs cultured in hAS and FBS we show that the *in vitro* molecular signature associated with hAS induced identity and potency can be used to develop defined culture conditions for hPDC culture. Furthermore, these culture conditions can be combined with high density collagen 3D matrices to promote periosteum-like tissue formation *in vitro*. Indeed, mimicking the periosteum microenvironment as a means of facilitating bone regeneration *in vivo*, is a credible method of introducing cells into bone defects that lack the key components to initiate the repair process.

Serum contains over 1,000 different components, including proteins, lipids, carbohydrates, growth factors, enzymes and other constituents that are still undefined. The precise effect of serum is cell type specific, however, generally it regulates cell growth and phenotype. As previously stated, we have shown that serum from human sources outperforms those from bovine sources when culturing hPDCs, however the mechanism of this effect and factors that mediate it are largely unexplored. Indeed, although EGF, FGF-2, PDGF, VEGF and IGF-1 have been identified as key growth factors in human serum (32), whether all or only some confer hPDC identity and potency is unknown. Interestingly, 4 of

these factors are represented in the 9 factors identified from transcriptomic analysis of hAS cultured hPDCs (PDGF-BB, β-estradiol, WNT3A, IGF-1, TNFα, TGFβ, VEGF, FGF2 and Dexamethasone). Furthermore, each of these 9 factors have also been implemented in stem cell culture and increased potency. There is already a wealth of literature suggesting these factors are important in: 1. Delaying MSC senescence (Oestrogen and Dexamethasone) (33)(34)(33); 2. Improving proliferation (Oestrogen, Dexamethasone, PDGF, Wnt3a, VEGF, and FGF) (36)(37)(38)(39) and 3. Regulating osteo/chondro commitment (TNF, TGFβ, IGF) (40)(41)(42)(38). Involvement of each of the selected factors in stem cell/bone biology is summarised in Supplementary Table 4. Of course, the validity of each of these factors for increasing hPDC potency, and potential interactions, requires careful testing empirically.

In an attempt to create a cocktail of growth factors that stimulate robust expansion of hPDCs with improved potency, a take-one-away methodology was used. It was predicted that when analysed with respect to cell proliferation and gene expression profile, a conclusion on the specific factor's importance could be made. For example, the inclusion of Wnt-3a in the initial growth factor list was predominantly a result of its significance as an upstream regulator in the transcriptomic analysis and previous studies indicating its role in bone metabolism and MSC proliferation. However, studies have reported contradictory results with regards to Wnt3a and osteocommitment, which appears to be dependent of cell type and stage of differentiation. Indeed, when considering adipose derived MSCs, Wnt3A increased the early marker ALP, but mature osteoblast markers were not increased (43). Conversely, a positive effect on multipotent characteristics and proliferative state has been suggested for bone marrow MSCs when FGF2 and Wnt3a care combined (44). Nevertheless, herein, eliminating Wnt-3a had a positive effect on cell proliferation but no effect on any stem or osteochondrogenic markers.

The elimination of Dexamethasone resulted in a significant upregulation of all tested gene markers (with the exception of ALP) as well as enhancing cellular proliferation and metabolism. Due to its dose dependent mechanism, Dexamethasone has previously been reported to both promote and arrest osteogenic differentiation. Interestingly herein, Dexamethasone appeared to have a negative effect on hPDC biology. Indeed, we have previously reported that Dexamethasone overall has a negative effect on osteogenic differentiation, unless in combination with 10% FBS (45). Likewise, eliminating VEGF from culture resulted in minimal alteration in analysed markers, but did promote proliferation and metabolism relative to all factors. VEGF is known to promote osteogenic differentiation, however, a lack of effect when considering PDCs may represent a cell specific mechanistic difference. In summary, eliminating a combination of Wnt-3a, Dex and VEGF had minimal negative effect in the cell's stem, osteogenic and chondrogenic markers relative to all other factors with the cell's morphology resembling that of cells cultured in hAS. This allowed the formulation of the defined PD-GFC culture conditions.

A significant difference was observed in the proliferation of cells cultured in PD-GFC relative to FBS, as previously reported with hAS (11). In addition, cell morphology and spreading of hPDCs cultured in PD-GFC mimicked that of cells cultured in hAS (11). Furthermore, hPDCs cultured in PD-GFC demonstrated significant increases in stem cell markers *PRX1* and *NESTIN* over serial passages and an increase in the chondrocyte marker *COL2A1* and osteogenic marker *RUNX2*. When expanded in PD-GFC, the resultant cells had a greater propensity to deposit GAGs when differentiated towards chondrocytes, and a decrease in fat droplet content when differentiated towards adipocytes, compared to cells cultured in 10% FBS. Indeed, this mirrored the results with hAS, with the exception of CaP deposition where an increase was observed compared to FBS (46). However, hPDC optimised osteogenic differentiation conditions were used herein, which were not used in the earlier study. Interestingly, periostin (POSTN) has been proposed as a key regulator of the cell's differentiation capacity (47). Indeed, culturing hPDCs in the PD-GFC caused a significant up regulation of *POSTN* (not shown) compared to FBS cultured cells, which may account in part for the enhanced differentiation capacity of the cells.

In an attempt to further mimic the periosteum *in vitro*, the cells were incorporated within a collagen type-1 matrix. Interestingly, we observed a distinct migration of cells to the fluid leaving surface of the collagen scaffold by day 14 (illustrated on the bottom edge of the collagen scaffolds in Figure 5B) when culturing the cells in PD-GFC. This resembled the cell distribution seen in native periosteum where cell density is increased in the cambium layer of the periosteum (as illustrated in Figure 5A). A significant increase in expression (***, $p<0.001$) of the periosteum associated gene cathepsin K (CTSK) (data not shown), was seen in scaffolds cultured in PD-GFC relative to FBS by day 14. CTSK is a collagenase enzyme that has recently been shown to be expressed in a subpopulation of periosteal stem cells (6), however in this instance it may be aiding matrix remodelling, thus allowing cell movement. In an attempt to define the cues relating to cell movement we assessed whether matrix stiffness was regulating migration. Interestingly, no difference was observed between the stiffness of the two surfaces of the scaffold, although they were in the same stiffness range as native periosteum. However, upon analysis of collagen orientation of both the scaffold and periosteum, a similar interwoven morphology was observed between the cambium layer and FLS of the scaffold. Additionally, a similar longitudinally oriented collagen fibre morphology was observed between the fibrous layer and bottom of the scaffold. As such, the matrix ultrastructure could be a potential cue in regulating the migration of cells to the various regions of the scaffold. Indeed, contact guidance and bidirectional migration along aligned collagen fibres is a known phenomenon in both wound healing and cancer biology (48). The increased population of hPDCs at the FLS when cultured in the PD-GFC suggests a synergistic effect of the dense interwoven collagen matrix as well as the presence of active cytokines and growth factors that may have encouraged the accumulation of PDCs. This pattern and localisation of cells in a collagen matrix is reminiscent of the cambium layer of the periosteum.

When assessing the signalling transduction pathways associated with the aforementioned culture system, down regulated pathways were predominantly associated with the TGF-β and Wnt, and upregulated pathways associated with CREB. Interestingly, upregulated genes include EP300 and CREB Binding Protein (CREBBP). EP300 is a histone acetyltransferase and coactivator and plays a vital role in physiological processes including the regulation of embryonic stem cell self-renewal and pluripotency (49). The homologous genes CREBBP and EP300 are recruited by Nanog (an identified hub gene) through a physical interaction to the Nanog binding loci and play a pivotal role in maintaining a proliferative and undifferentiated population of stromal stem cells (50). Additionally, CREB-mediated signalling has been implicated in the expansion and self-renewal of muscle stem cells to preserve stem cell function (51). Interestingly, CREB has also been linked with *in vivo* bone formation, with prolonged activation of the cAMP pathway by either dibutryl-cAMP (52) or forskolin (53) shown to stimulate *in vitr*o and *in vivo* bone formation from human MSCs. Furthermore, CREB is linked to periosteal biology. Indeed, PDGF secreted by TRAP^{+} mononuclear cells have been shown to maintain the periosteum microenvironment potentially though its induction of pCREB binding to the periostin promoter (54).

As previously mentioned, an overall decrease in WNT signalling was apparent in cells cultured in the PD-GFC relative to FBS. With reference to the initial take-one-away study, the presence of WNT3a had a negative effect on cell proliferation and as such was eliminated from further analysis. Interestingly, the six growth factors selected in addition to the 3D matrix induced an autonomous downregulation of WNT signalling, further highlighting the need to eliminate this pathway. Indeed, it is known that activation of WNT signalling leads to periosteal bone formation, presumably as a direct result of periosteal stem cell differentiation (55). TGF-β signalling was also down-regulated in this system. Specifically, the type 1 receptor ACVR1B and the type 2 receptor ACVR2B was downregulated. These two receptors form the signalling complex for activins including Activin a, Activin b and Nodal. This signalling pathway functions through the interaction of Smad2/3 with Smad4, which is also downregulated in our analysis. Interestingly, Activin/Nodal signalling has been implicated in both pluripotent and adult stem cell fate choices (56).

Overall, the PD-GFC developed in the current study represents a defined media for the expansion of hPDCs *in vitro,* whilst retaining cell identity and improving potency. Incorporating PD-GFC cultured cells in a collagen type-1 matrix mimicked native periosteum through cell localisation. Regulation of specific pathways in response to PD-GFC and the environment suggest the enrichment or modification of hPDCs to mimic the periosteal progenitor niche. These data could provide the basis for an 'off the shelf' periosteum mimetic to replace periosteal grafting *in vivo*, however, efficacy of such a construct would firstly need to be tested preclinically.

References

1. Lin Z, Fateh A, Salem DM, Intini G. Periosteum: biology and applications in craniofacial bone regeneration. J Dent Res [Internet]. 2014 Feb [cited 2018 Jul 30];93(2):109–16.
2. Ito Y, Fitzsimmons JS, Sanyal A, Mello MA, Mukherjee N, O'driscoll SW. Localization of chondrocyte precursors in periosteum. Osteoarthr Cartil. 2001.
3. Dwek JR. The periosteum: what is it, where is it, and what mimics it in its absence? Skeletal Radiol. 2010;39(4):319.
4. Evans SF, Chang H, Knothe Tate ML. Elucidating Multiscale Periosteal Mechanobiology: A Key to Unlocking the Smart Properties and Regenerative Capacity of the Periosteum? Tissue Eng Part B Rev. 2012.
5. Knothe UR, Dolejs S, Matthew Miller R, Knothe Tate ML. Effects of mechanical loading patterns, bone graft, and proximity to periosteum on bone defect healing. J Biomech. 2010.
6. Debnath S, Yallowitz AR, McCormick J, Lalani S, Zhang T, Xu R, et al. Discovery of a periosteal stem cell mediating intramembranous bone formation. Nature. 2018.
7. Roberts SJ, van Gastel N, Carmeliet G, Luyten FP. Uncovering the periosteum for skeletal regeneration: The stem cell that lies beneath. Bone [Internet]. 2015;70:10–8.
8. Petrochenko P, Narayan RJ. Novel Approaches to Bone Grafting: Porosity, Bone Morphogenetic Proteins, Stem Cells, and the Periosteum. J Long Term Eff Med Implants. 2012.
9. Geris L, Reed AAC, Vander Sloten J, Simpson AHRW, Van Oosterwyck H. Occurrence and Treatment of Bone Atrophic Non-Unions Investigated by an Integrative Approach. Bourne PE, editor. PLoS Comput Biol [Internet]. 2010 Sep 2 [cited 2019 Mar 18];6(9):e1000915.
10. Knothe UR, Springfield DS. A novel surgical procedure for bridging of massive bone defects. World J Surg Oncol. 2005.
11. Roberts SJ, Owen HC, Tam WL, Solie L, Van Cromphaut SJ, Van den Berghe G, et al. Humanized culture of periosteal progenitors in allogeneic serum enhances osteogenic differentiation and in vivo bone formation. Stem Cells Transl Med [Internet]. 2014 Feb [cited 2016 Feb 11];3(2):218–28.
12. Colnot C. Skeletal Cell Fate Decisions Within Periosteum and Bone Marrow During Bone Regeneration. J Bone Miner Res [Internet]. 2009 Feb [cited 2016 Sep 25];24(2):274–82.
13. Roberts SJ, Geris L, Kerckhofs G, Desmet E, Schrooten J, Luyten FP. The combined bone forming capacity of human periosteal derived cells and calcium phosphates. Biomaterials [Internet]. 2011 Jul [cited 2016 Jan 31];32(19):4393–405.
14. De Bari C, Dell'Accio F, Vanlauwe J, Eyckmans J, Khan IM, Archer CW, et al. Mesenchymal multipotency of adult human periosteal cells demonstrated by single-cell lineage analysis. Arthritis Rheum [Internet]. 2006 Apr [cited 2016 Jan 2];54(4):1209–21.
15. Cimino M, Gonçalves RM, Barrias CC, Martins MCL. Xeno-Free Strategies for Safe Human Mesenchymal Stem/Stromal Cell Expansion: Supplements and Coatings. Stem Cells Int [Internet]. 2017 [cited 2019 Mar 13];2017:6597815.
16. Bjare U. Serum-free cell culture. Pharmacology and Therapeutics. 1992.
17. Zheng X, Baker H, Hancock WS, Fawaz F, McCaman M, Pungor E. Proteomic analysis for the assessment of different lots of fetal bovine serum as a raw material for cell culture. Part IV. Application of proteomics to the manufacture of biological drugs. Biotechnol Prog. 2006.
18. Simonetti AB, Englert GE, Campos K, Mergener M, David C de, Oliveira AP de, et al.

Nanobacteria-like particles: a threat to cell cultures. Brazilian J Microbiol [Internet]. 2007 Mar [cited 2019 Mar 18];38(1):153–8.

19. Van Der Valk J, Mellor D, Brands R, Fischer R, Gruber F, Gstraunthaler G, et al. The humane collection of fetal bovine serum and possibilities for serum-free cell and tissue culture. In: Toxicology in Vitro. 2004.

20. Brunner D, Frank J, Appl H, Schöffl H, Pfaller W, Gstraunthaler G. Serum-free cell culture: the serum-free media interactive online database. ALTEX. 2010.

21. Gupta P, Hall GN, Geris L, Luyten FP, Papantoniou I. Human Platelet Lysate Improves Bone Forming Potential of Human Progenitor Cells Expanded in Microcarrier-Based Dynamic Culture. Stem Cells Transl Med. 2019.

22. Van der Valk J, Bieback K, Buta C, Cochrane B, Dirks WG, Fu J, et al. Fetal Bovine Serum (FBS): Past - Present - Future. ALTEX. 2018.

23. Chen Y, Sonnaert M, Roberts SJ, Luyten FP, Schrooten J. Validation of a PicoGreen-based DNA quantification integrated in an RNA extraction method for two-dimensional and three-dimensional cell cultures. Tissue Eng Part C Methods [Internet]. 2012 Jun 1 [cited 2016 Apr 22];18(6):444–52.

24. Livak KJ, Schmittgen TD. Analysis of relative gene expression data using real-time quantitative PCR and the 2(-Delta Delta C(T)) Method. Methods. 2001.

25. Chen C, Luyten F, Schrooten J, Eyckmans J, Roberts S. Growth Factor Cocktail To Enhance Osteogenic Differentiation Of Mesenchymal Cells - Patent application [Internet]. Patentdocs. 20150307846, 2015 [cited 2016 Jan 30].

26. Magdeldin T, López-Dávila V, Pape J, Cameron GWW, Emberton M, Loizidou M, et al. Engineering a vascularised 3D in vitro model of cancer progression. Sci Rep [Internet]. 2017 Dec 9 [cited 2018 Dec 11];7(1):44045.

27. Hadjipanayi E, Ananta M, Binkowski M, Streeter I, Lu Z, Cui ZF, et al. Mechanisms of structure generation during plastic compression of nanofibrillar collagen hydrogel scaffolds: Towards engineering of collagen. J Tissue Eng Regen Med. 2011.

28. Brown RA, Wiseman M, Chuo CB, Cheema U, Nazhat SN. Ultrarapid engineering of biomimetic materials and tissues: Fabrication of nano- and microstructures by plastic compression. Adv Funct Mater. 2005.

29. Rio DC, Ares M, Hannon GJ, Nilsen TW. Purification of RNA using TRIzol (TRI Reagent). Cold Spring Harb Protoc. 2010.

30. Méndez-Ferrer S, Michurina T V., Ferraro F, Mazloom AR, MacArthur BD, Lira SA, et al. Mesenchymal and haematopoietic stem cells form a unique bone marrow niche. Nature. 2010.

31. Ouyang Z, Chen Z, Ishikawa M, Yue X, Kawanami A, Leahy P, et al. Prx1 and 3.2kb Col1a1 promoters target distinct bone cell populations in transgenic mice. Bone. 2014.

32. Montali M, Barachini S, Panvini FM, Carnicelli V, Fulceri F, Petrini I, et al. Growth Factor Content in Human Sera Affects the Isolation of Mesangiogenic Progenitor Cells (MPCs) from Human Bone Marrow. Front Cell Dev Biol [Internet]. 2016 Oct 17 [cited 2019 Aug 29];4:114.

33. Hong L, Zhang G, Sultana H, Yu Y, Wei Z. The effects of 17-β estradiol on enhancing proliferation of human bone marrow mesenchymal stromal cells in vitro. Stem Cells Dev [Internet]. 2011 May [cited 2016 Apr 11];20(5):925–31.

34. Yun SP, Lee MY, Ryu JM, Song CH, Han HJ. Role of HIF-1alpha and VEGF in human mesenchymal stem cell proliferation by 17beta-estradiol: involvement of PKC, PI3K/Akt, and MAPKs. Am J Physiol Cell Physiol [Internet]. 2009 Feb 1 [cited 2016 Apr 12];296(2):C317-26.

35. Xiao Y, Peperzak V, van Rijn L, Borst J, de Bruijn J. Dexamethasone treatment during the expansion phase sustains stemness of mesenchymal stem cells from human bone marrow. Cell Res [Internet]. 2008 Aug [cited 2016 Apr 14];18(S1):S116–S116.

36. De Boer J, Wang HJ, Van Blitterswijk C. Effects of Wnt signaling on proliferation and differentiation of human mesenchymal stem cells. Tissue Eng. 2004;10(3–4):393–401.

37. Lienemann PS, Devaud YR, Reuten R, Simona BR, Karlsson M, Weber W, et al. Locally controlling

mesenchymal stem cell morphogenesis by 3D PDGF-BB gradients towards the establishm

38.   Huang Z, Ren P-G, Ma T, Smith RL, Goodman SB. Modulating osteogenesis of mesenchymal stem cells by modifying growth factor availability. Cytokine [Internet]. 2010 Sep [cited 2016 Apr 7];51(3):305–10.

39.   Ahn H-J, Lee W-J, Kwack K, Kwon Y Do. FGF2 stimulates the proliferation of human mesenchymal stem cells through the transient activation of JNK signaling. FEBS Lett [Internet]. 2009 Sep 3 [cited 2016 Apr 11];583(17):2922–6.

40.   Croes M, Oner FC, Kruyt MC, Blokhuis TJ, Bastian O, Dhert WJA, et al. Proinflammatory Mediators Enhance the Osteogenesis of Human Mesenchymal Stem Cells after Lineage Commitment. PLoS One [Internet]. 2015 Jan 15 [cited 2016 Mar 7];10(7):e0132781.

41.   Ng F, Boucher S, Koh S, Sastry KSR, Chase L, Lakshmipathy U, et al. PDGF, TGF-beta, and FGF signaling is important for differentiation and growth of mesenchymal stem cells (MSCs): transcriptional profiling can identify markers and signaling pathways important in differentiation of MSCs into adipogenic, chondrogenic, and o. Blood [Internet]. 2008 Jul 15 [cited 2016 Mar 7];112(2):295–307.

42.   Minuto F, Palermo C, Arvigo M, Barreca AM. The IGF system and bone. [Internet]. Vol. 28, Journal of endocrinological investigation. 2005. p. 8–10.

43.   Batsali AK, Pontikoglou C, Koutroulakis D, Pavlaki KI, Damianaki A, Mavroudi I, et al. Differential expression of cell cycle and WNT pathway-related genes accounts for differences in the growth and differentiation potential of Wharton's jelly and bone marrow-derived mesenchymal stem cells. Stem Cell Res Ther [Internet]. 2017 [cited 2019 Aug 29];8(1):102.

44.   Narcisi R, Cleary MA, Brama PAJ, Hoogduijn MJ, Tüysüz N, Ten Berge D, et al. Long-term expansion, enhanced chondrogenic potential, and suppression of endochondral ossification of adult human MSCs via WNT signaling modulation. Stem Cell Reports. 2015.

45.   Roberts SJ, Chen Y, Moesen M, Schrooten J, Luyten FP. Enhancement of osteogenic gene expression for the differentiation of human periosteal derived cells. Stem Cell Res [Internet]. 2011 Sep [cited 2016 Mar 4];7(2):137–44.

46.   Eyckmans J, Roberts SJ, Bolander J, Schrooten J, Chen CS, Luyten FP. Mapping calcium phosphate activated gene networks as a strategy for targeted osteoinduction of human progenitors. Biomaterials [Internet]. 2013 Jun [cited 2016 Feb 1];34(19):4612–21.

47.   Duchamp de Lageneste O, Julien A, Abou-Khalil R, Frangi G, Carvalho C, Cagnard N, et al. Periosteum contains skeletal stem cells with high bone regenerative potential controlled by Periostin. Nat Commun [Internet]. 2018 Dec 22 [cited 2018 Jul 6];9(1):773.

48.   Wang J, Koelbl J, Boddupalli A, Yao Z, Bratlie KM, Schneider IC. Transfer of assembled collagen fibrils to flexible substrates for mechanically tunable contact guidance cues. Integr Biol (United Kingdom). 2018.

49.   Fang F, Chew K, Chen X, Matsudaira P. Coactivators p300 and CBP Maintain the Identity of Mouse Embryonic Stem Cells by Mediating Long-Range Chromatin Structure. Stem Cells [Internet]. 2014 [cited 2019 Aug 29];32:1805–16.

50.   Tsai C-C, Hung S-C. Functional roles of pluripotency transcription factors in mesenchymal stem cells. Cell Cycle [Internet]. 2012 Oct 15 [cited 2019 Aug 29];11(20):3711–2.

51.   Li L, Fan CM. A CREB-MPP7-AMOT Regulatory Axis Controls Muscle Stem Cell Expansion and Self-Renewal Competence. Cell Rep. 2017.

52.   Siddappa R, Martens A, Doorn J, Leusink A, Olivo C, Licht R, et al. cAMP/PKA pathway activation in human mesenchymal stem cells in vitro results in robust bone formation in vivo. Proc Natl Acad Sci U S A [Internet]. 2008 May 20 [cited 2016 Jan 26];105(20):7281–6.

53.   Doorn J, Siddappa R, van Blitterswijk CA, de Boer J. Forskolin Enhances *In Vivo* Bone Formation by Human Mesenchymal Stromal Cells. Tissue Eng Part A [Internet]. 2012 Mar 31 [cited 2019 Aug 29];18(5–6):558–67.

54.   Gao B, Deng R, Chai Y, Chen H, Hu B, Wang X, et al. Macrophage-lineage TRAP+ cells recruit periosteum-derived cells for periosteal osteogenesis and regeneration. J Clin Invest. 2019.

55. Bolander J, Chai YC, Geris L, Schrooten J, Roberts SJ, Luyten FP. Early BMP, Wnt and Ca2+/PKC Pathway Activation Predicts the Bone Forming Capacity of Periosteal Cells in Combination with Calcium Phosphates. Biomaterials [Internet]. 2016 Jan [cited 2016 Jan 31].

56. Pauklin S, Vallier L. Activin/nodal signalling in stem cells. Development (Cambridge). 2015.

57. Wang Q, Yu J, Zhai H, Zhao Q, Chen J, Shu L, et al. Temporal expression of estrogen receptor alpha in rat bone marrow mesenchymal stem cells. Biochem Biophys Res Commun [Internet]. 2006 Aug 18 [cited 2016 Apr 11];347(1):117–23.

58. Yun SP, Lee MY, Ryu JM, Song CH, Han HJ. Role of HIF-1alpha and VEGF in human mesenchymal stem cell proliferation by 17beta-estradiol: involvement of PKC, PI3K/Akt, and MAPKs. Am J Physiol Cell Physiol [Internet]. 2009 Feb 1 [cited 2016 Apr 12];296(2):C317-26.

59. Chen F-P, Hu C-H, Wang K-C. Estrogen modulates osteogenic activity and estrogen receptor mRNA in mesenchymal stem cells of women. Climacteric [Internet]. 2013 Feb [cited 2016 Apr 11];16(1):154–60.

60. Chang J-K, Ho M-L, Yeh C-H, Chen C-H, Wang G-J. Osteogenic gene expression decreases in stromal cells of patients with osteonecrosis. Clin Orthop Relat Res [Internet]. 2006 Dec [cited 2016 Mar 21];453:286–92.

61. Hong L, Sultana H, Paulius K, Zhang G. Steroid regulation of proliferation and osteogenic differentiation of bone marrow stromal cells: a gender difference. J Steroid Biochem Mol Biol [Internet]. 2009 Apr [cited 2016 Apr 14];114(3–5):180–5.

62. Xiao Y, Peperzak V, van Rijn L, Borst J, de Bruijn JD. Dexamethasone treatment during the expansion phase maintains stemness of bone marrow mesenchymal stem cells. J Tissue Eng Regen Med [Internet]. 2010 Jul [cited 2016 Apr 14];4(5):374–86.

63. Langenbach F, Handschel J. Effects of dexamethasone, ascorbic acid and β-glycerophosphate on the osteogenic differentiation of stem cells in vitro. Stem Cell Res Ther [Internet]. 2013 Jan [cited 2016 Apr 14];4(5):117.

64. Kwon YW, Heo SC, Jeong GO, Yoon JW, Mo WM, Lee MJ, et al. Tumor necrosis factor-α-activated mesenchymal stem cells promote endothelial progenitor cell homing and angiogenesis. Biochim Biophys Acta [Internet]. 2013 Dec [cited 2016 Feb 10];1832(12):2136–44.

65. Egea V, von Baumgarten L, Schichor C, Berninger B, Popp T, Neth P, et al. TNF-α respecifies human mesenchymal stem cells to a neural fate and promotes migration toward experimental glioma. Cell Death Differ [Internet]. 2011 May [cited 2016 Mar 7];18(5):853–63.

66. Yokota J, Chosa N, Sawada S, Okubo N, Takahashi N, Hasegawa T, et al. PDGF-induced PI3K-mediated signaling enhances the TGF-β-induced osteogenic differentiation of human mesenchymal stem cells in a TGF-β-activated MEK-dependent manner. Int J Mol Med [Internet]. 2014 Mar 1 [cited 2016 Apr 28];33(3):534–42.

67. Liu G, Vijayakumar S, Grumolato L, Arroyave R, Qiao H, Akiri G, et al. Canonical Wnts function as potent regulators of osteogenesis by human mesenchymal stem cells. J Cell Biol. 2009;185(1):67–75.

68. Boland GM, Perkins G, Hall DJ, Tuan RS. Wnt 3a promotes proliferation and suppresses osteogenic differentiation of adult human mesenchymal stem cells. J Cell Biochem [Internet]. 2004 Dec 15 [cited 2016 Apr 7];93(6):1210–30.

69. Liu Y, Berendsen AD, Jia S, Lotinun S, Baron R, Ferrara N, et al. Intracellular VEGF regulates the balance between osteoblast and adipocyte differentiation. J Clin Invest [Internet]. 2012 Sep [cited 2016 Apr 7];122(9):3101–13.

70. Berendsen AD, Olsen BR. How vascular endothelial growth factor-A (VEGF) regulates differentiation of mesenchymal stem cells. J Histochem Cytochem [Internet]. 2014 Feb [cited 2016 Apr 7];62(2):103–8.

71. Schönmeyr BH, Soares M, Avraham T, Clavin NW, Gewalli F, Mehrara BJ. Vascular endothelial growth factor inhibits bone morphogenetic protein 2 expression in rat mesenchymal stem cells. Tissue Eng Part A [Internet]. 2010 Feb [cited 2016 Apr 7];16(2):653–62.

72.	Jian H, Shen X, Liu I, Semenov M, He X, Wang X-F. Smad3-dependent nuclear translocation of beta-catenin is required for TGF-beta1-induced proliferation of bone marrow-derived adult human mesenchymal stem cells. Genes Dev [Internet]. 2006 Mar 15 [cited 2016 Apr 16];20(6):666–74.

73.	Choi S-C, Kim S-J, Choi J-H, Park C-Y, Shim W-J, Lim D-S. Fibroblast growth factor-2 and -4 promote the proliferation of bone marrow mesenchymal stem cells by the activation of the PI3K-Akt and ERK1/2 signaling pathways. Stem Cells Dev [Internet]. 2008 Aug [cited 2016 Apr 11];17(4):725–36.

74.	Doorn J, Roberts SJ, Hilderink J, Groen N, van Apeldoorn A, van Blitterswijk C, et al. Insulin-Like Growth Factor-I Enhances Proliferation and Differentiation of Human Mesenchymal Stromal Cells In Vitro. Tissue Eng Part A [Internet]. 2013;19:1817–28.

Validation of RNA SEQ Gene Expression
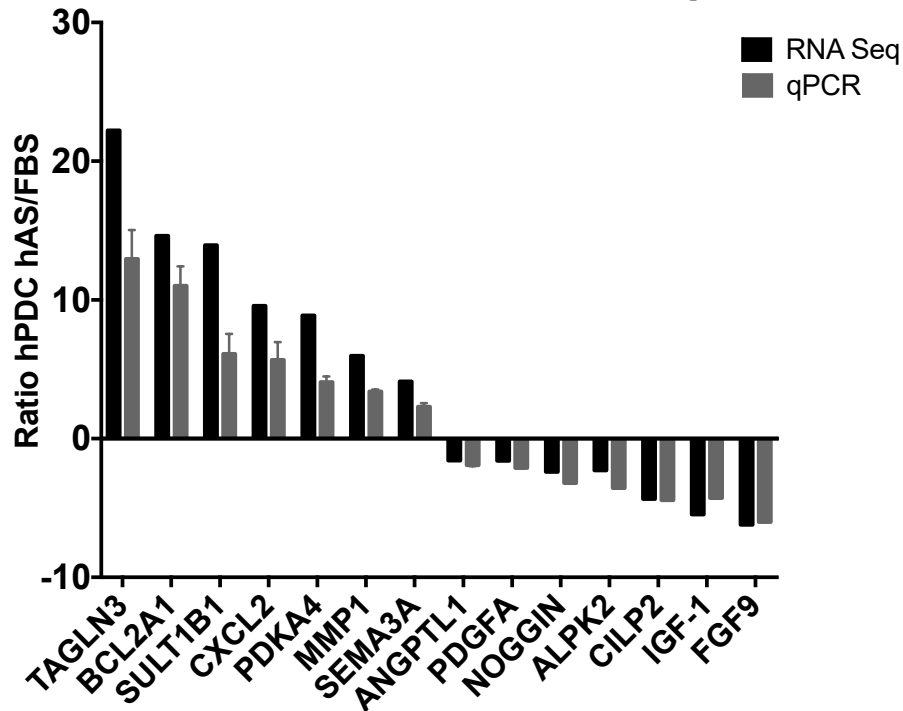
Supplementary Figure 1: Validation of RNA Sequencing
Validation of RNA Seq data was performed on RNA obtained from the hPDCs cultured in 10% hAS or FBS using qPCR. The selected genes were based on RNA Seq fold changes (highly up or down regulated (fold change >20), moderate regulation (fold change of 10-20) and low up and down regulated (fold change >20)) in cells cultured in hAS (n=3) compared to FBS (n=3). Data are presented as the ratio of cells cultured in 10% FBS/ 10% hAS. Minimal fold change differences in gene expression were observed between the RNA Seq obtained data and the validation qPCR (Data are presented as the mean ±S.E.M).
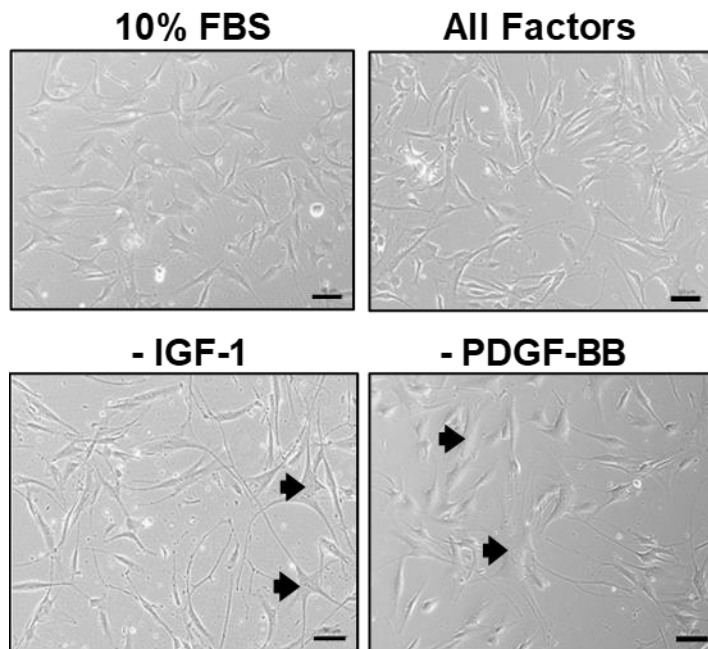
Supplementary Figure 2: hPDC morphology following removal of IGF-1 and PDGF-BB
Light microscopic images of hPDCs cultured the absence of IGF-1 and PDGF-BB showing an induction of a heterogeneous culture and or stress fibers compared to all factor or FBS culture (indicated by arrows; Scale bar: 50 μm).
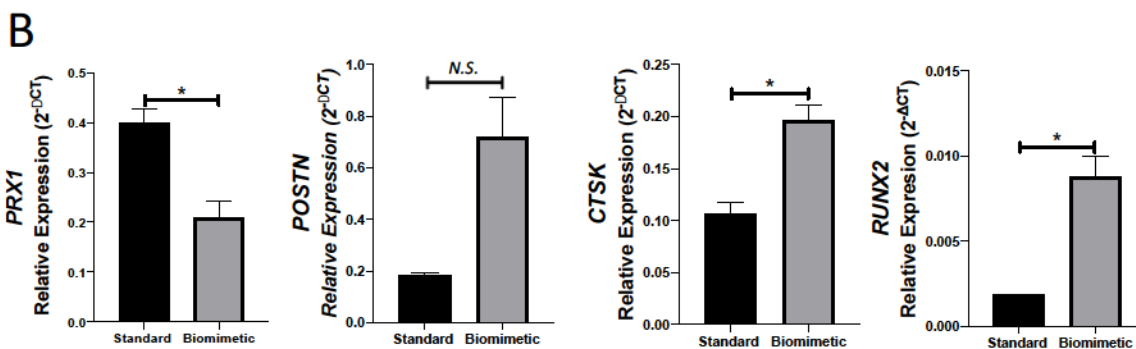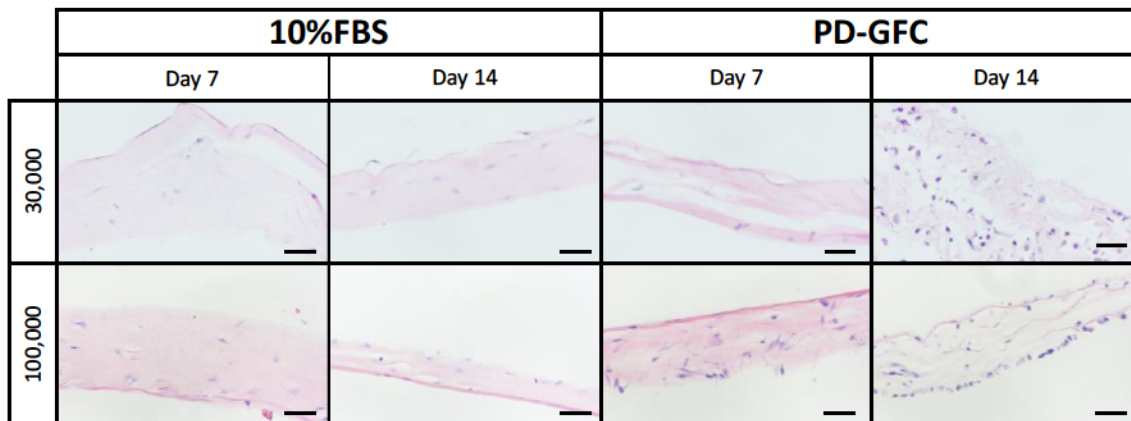
Supplementary Figure 3: Cell density modulates migration of hPDCs to the FLS with 100,000 cells replicating aspects of periosteal biology. (A) Histological (H&E) images of hPDCs cultured in FBS or PD-GFC for 7 or 14 days at either 30,000 or 100,00 cells per gel (21.76 mm^3). Note cell organization along one surface at the 100,000-cell density, cultured in PD-GFC at Day 14 (Scale bar: 50 μm). **(B)** Gene expression of key genes associated with periosteal biology in cells cultured in standard vs biomimetic (100,000-cell density, cultured in PD-GFC at Day 14 in plastic-compressed gels; Data are presented as the mean ±S.E.M, Statistical analysis performed using one-way ANOVA, uncorrected Fischer's LSD; *p<0.05; n=3).

Supplementary Table 1

Gene Name	Forward (5'-3')	Reverse (3'-5')
BCL2A1	ACACAGGAGAATGGATAAGGC	TCAACAGTATTGCTTCAGGAGAG
SULT1B1	TGGCTCGTAATGCCAAGGAT	ACCATAGGCCACTTTTCCAGTT
CXCL2	CTCTCCTCCTCGCACAGC	GGGCGCTCCTGCTGC
PDK4	GTGATGTGGTAGCAGTGGTC	GGTGAGAAGGAACATACACGATG
TAGLN3	AGTTCCTAAAAGCTGCGGAG	TCATCCTTGGTGACTGCAAC
MMP1	TGTGGTGTCATCACAGCTTCC	GGGCCACTATTTCTCCGCTT
SEM3A	AAAGCGTGTGCTGAGTGTTG	TTGTCGTCTTGTGCGTCTCT
ANGPTL1	TGTATGCAGGAAACTGCGCC	TTGCTTCTGTAATGGCCTCCTC
PDGFA	CCTGGAGATAGACTCCGTAGG	GCTTCCTCGATGCTTCTCTTC
NOGGIN	CAGTACCCCATCATTTCCGAG	TCATTGAAAACCCTCGCTAGAG
ALPK4	AACGCTGGCTAAAGGGTACA	GGCTGCTTCTGTTTCTGGTTG
CILP2	ACCTGGTGAAACACCCTGAG	CCCATTGTGGAACCAGGAGTA
IGF-1	CTTCAGTTCGTGTGTGGAGACA	CGCCCTCCGACTGCTG
FGF9	GGGGAGCTGTATGGATCAGAAA	GTATCGCCTTCCAGTGTCCA

Primer sequences for RT-PCR. Primers used for validation of RNA SEQ data.

Gene Name C	Forward (5'-3')	Reverse (3'-5')
NES	GGCCACGTACAGGACCCTC	CCTCTGGGGTCCTAGGGAAT
PRX1	CGAGAGTGCAGGTGTGGTTT	GAGCAGGACGAGGTACGAT
RUNX2	CGCATTCCTCATCCCAGTAT	GCCTGGGGTCTGTAATCTGA
ALP	GGACATGCAGTACGTAGCTGA	GTCAATTCTGCCTCCTTCCA
COL2A1	CTCCGTCAAGTCCGAGCA	ACGGCTGACAAGGCCACA
SOX9	TGGAGACTTCTGAACGAGAGC	CGTTCTTCACCGACTTCCTC
FABP4	CATACTGGGCCAGGAATTTG	GGACACCCCCTCTAAGGTT
POSTN	GGTCCTAATTCCTGATTCTGCC	CCAGCAAAGTGTATTCTCCATC
COL1A1	CCCTGTCTGCTTCCTGTAAAC	AGTCCATGTGAAATTGTCTCCC

Primer sequences for cell analysis.

Supplemetary Table 2

Upstream Regulator	p-value of overlap
β-estradiol	$8.89E^{-18}$
Dexamethasone	$1.15E^{-16}$
TGFB1	$7.21E^{-14}$
TNF	$8.69E^{-13}$
PDGF BB	$2.70E^{-12}$
IL1β	$2.75E^{-12}$
Ni2+	$3.35E^{-12}$
F2	$1.22E^{-11}$
Triamcinolone Acetonide	$4.26E^{-11}$
NFkB (complex)	$4.79E^{-11}$
Progesterone	$1.36E^{-10}$
TREM1	$1.46E^{-10}$
MEOX2	$4.67E^{-10}$
IL17F	$6.82E^{-10}$
WNT3A	$8.65E^{-10}$
Cycloheximide	$1.06E^{-09}$
Tgf-β	$1.22E^{-09}$
S100A8	$1.34E^{-09}$
IFNG	$1.40E^{-09}$
Simvastatin	$1.56E^{-09}$

List of upstream transcriptional regulators identified using IPA. They are listed in order of their p-value of overlap. Overlap p-value is used to identify transcriptional regulators that may explain observed gene expression changes.

Supplementary Table 3

Network	Hub Genes
1) Cancer, Organismal Injury and Abnormalities, Gastrointestinal Disease	Akt, MYOC, Integrin, TRIB3
2) Cancer, Gastrointestinal Disease, Organismal Injury and Abnormalities	ERK, FGFR2, Rb, FGF9, HDAC, Cyclin E, Cyclin A, E2f
3) Cellular Movement, Hematological System Development and Function, Hypersensitivity Response	VCAM1, Rac, GSK3, LEF1, p85
4) Embryonic Development, Organismal Development, Tissue Development	IGF1, MApk, IGF2, VEGF, CDH1, MAPK1/2, TNFRS11B
5) Cellular Movement, Hematological System Development and Function, Immune Cell Trafficking	ERK 1/2, CTGF, MMP1, COll4, IL-17R, GREM1
6) Cellular Development, Cellular Growth and Proliferation, Hematological System Development and Function	NF-kB, Nfat, IgE, TNFSF4
7) Dermatological Diseases and Conditions, Organismal Injury and Abnormalities, Skeletal and Muscular System Development and Function	PDGF, PKc, TNF family, Pld, hsp27
8) Cancer, Organismal Injury and Abnormalities, Reproductive System Disease	RhoA, Tp53, NR3C1
9) Hereditary Disorder, Metabolic Disease, Organismal Injury and Abnormalities	EGFR, Cul3
10) Neurological Disease, Skeletal and Muscular Disorders, Psychological Disorders	Ras homolog, PLC, Ras, Adcy, p38 MAPK, NMDA

Hub genes identified in each of the top 10 networks generated by IPA. Each network is associated with a specific disease and/or biological process.

Supplementary Table 4

Upstream Regulators	Molecule Type	P-value of overlap	Target Molecules	Main Networks Involved	Evidence to support selection of upstream regulators
β-estradiol	Chemical - endogenous mammalian	8.89E-18	ACKR3,ACTC1,ADM2,AGT,BCL2A1,BIRC3,CCL20,CD274,CDH1,CDKN1C,CNN1,COLEC12,COMP,CRLF1,CTGF,CXCL2,CXCL3,CXCL8,CYP1B1,CYP26B1,DDIT4,DHRS9,DSCAM,EDN1,EGR2,FABP5,FGF9,FGFR2,FMOD,GIPC2,GREM1,H19,HGF,IGF1,IGF2,ITGA2,KCND3,KRT16,KRT7,KRT81,LMCD1,LUM,MMP1,NCF2,NUPR1,OXTR,PDK4,PPARGC1B,RGS2,SEMA3A,SEPT4,SERTAD4,SFRP2,SLC6A9,STC1,STC2,TFPI,THBD,THRB,TNFRSF11B,TNNT3,TTC39A,TTN,VCAM1,YPEL3	2,4,5,7	➤ Recent studies have shown that 17β-estradiol can effectively improve bone marrow- mesenchymal stem cell- (BM-MSC) proliferation in mice and rats (57)(33). ➤ Estrogen has been confirmed to enhance the differentiation potential of hMSCs and to up-regulate their telomerase activity as a means of preventing telomere shortening via ERα, thus, inhibiting senescence of MSC. Upon estrogen supplementation, hMSCs demonstrated a significant increase in their proliferative rate; the cells maintained the differentiation potential at concentrations ranging from 10^{-9} and 10^{-8} M (33)(58). ➤ 17β-estradiol can regulate and significantly improve MSC proliferation *in vitro*, effectively improving MSC numbers and differentiation capacity required for stem cell-based tissue engineering. However, (33), male and female donor MSC proliferation differs in the presence of 17β-estradiol. ➤ The above claims can be further confirmed by Chen, et al stating estrogens functional involvement in enhancing the osteogenic activity of MSCs and their differentiation into osteoblasts. This was established by an increase in osteocalcin and ALP expression in estrogen treated MSCs (59).
Dexamethasone	Chemical Drug	1.15E-16	ACKR3,ADAMTS15,AGT,AMIGO2,ANGPTL4,ANOS1,ASPN,B3GNT5,BCL2A1,BIRC3,CCL20,CDKN1C,CFHR1,COL11A1,COL15A1,COL4A1,COL4A3,CTGF,CXCL2,CXCL3,CXCL6,CXCL8,CYP1B1,DDIT4,EDN1,EDNRB,EGR2,ELN,FABP5,FKBP5,G0S2,GDF15,HGF,IGF1,IGF2,ITGA2,KLHL24,KRT7,MMP1,MXRA5,MYOC,NOV,OXTR,PCK2,PDK4,PIK3IP1,PRRG4,RASL11B,RGS2,S100P,SCD,SEMA5B,SULT1B1,TGFBI,THBD,TNFRSF11B,TSLP,VCAM1,ZBTB16,ZNF704	1,4,5,6,7	➤ Dexamethasone (Dex) is known to be able to exert multiple effects on the same cell population according to the concentration of Dex present around and within the cells system. hBM-MSCs cultured in a Dex concentration of 10^{-8} M has shown to negatively regulate the transcription of genes associated with apoptosis and differentiation, while genes implicated in cell proliferation were positively regulated by Dex. ➤ Dex improves the quality of hBM-MSCs as it delays senescence and maintains its differentiation potential (35). ➤ High concentrations of dex (10^{-6}-10^{-7} M) suppresses the proliferation of hMSC-like cells but not their differentiation. Other studies however, have shown that this concentration suppresses osteogenic differentiation, directing the cells towards an adipogenic lineage (60)(61).

					➢ A study carried out by (62) has shown that MSCs cultured in low doses of Dex during the expansion phase, maintain a higher proliferative potential then cells cultured in the absence of Dex over repeated passages. Cells become phenotypically stable upon passaging. ➢ Dex can also initiate osteogenesis via Wnt/ β-catenin canonical pathway and an alternative pathway- the MAPK phosphatase (MKP-1) causing the expression of osteocalcin, *BSP* and *RUNX2* (63). ➢ Overall, Dex can induce either differentiation or proliferation in a dose dependent manner.
TNFα	Cytokine	8.69E-13	ACKR3,AGT,ALDH3A1,ANGPTL4,BCL2A1,BIRC3,CCL20,CD274,CDH1,CNN1,COL15A1,COL4A3,CRLF1,CSF2RB,CTGF,CXCL2,CXCL3,CXCL5,CXCL6,CXCL8,CYP1B1,CYP26B1,EDN1,EDNRB,EGR2,FABP5,FGFR2,FOXF1,G0S2,GDF15,GFRA2,H19,HGF,IGF1,IGF2,IL21R,ITGA2,MMP1,NCF2,NOV,NR4A2,NUAK1,PAPPA,PCK2,PPARGC1B,RGS2,SCD,STAT4,TFPI,THBD,TNFRSF11B,TSLP,VCAM1	4,5,6	➢ Kwon, Y. W., et al (2013) investigated the expression of pro-angiogenic factors IL-6 and IL-8 on TNFα stimulated hMSCs (64). At a concentration of 10 ng/ml, TNFα cultured cells stimulated angiogenesis and tissue repair (in 48hrs) (64). ➢ Furthermore, hMSC were subjected to a range of TNFα concentrations, from 0.5-50 ng/mL, in a study carried out by Croes, M. et al (2015). Lower concentrations of 5 ng/mL demonstrated higher ALP activity compared to control, and highest calcium deposition, both at a concentration of 5 ng/mL (40). ➢ An additional study investigated the long term incubation of hMSCs with TNFα in the induction of a neural phenotype (65). The Cells were subjected to TNFα stimulation with either a concentration of 5 ng/mL or 50 ng/mL. The lower dose of the cytokine exhibited a stimulatory effect on cell division with a 2-fold increase. Overall, these findings indicate the need to utilise a low concentration of TNFα (65).
PDGF-BB	Complex	2.70E-12	ACKR3,CCL20,CNN1,CTGF,CXCL2,CXCL8,EDN1,EDNRB,EGR2,GDF15,GREM1,H19,IGF1,IGF2,MMP1,MYH1,NR4A2,RGS2,SCD,THBD,TRIB3,UNC5B,VCAM1	4, 5	➢ hMSCs cultured in a 3D polyethylene glycol (PEG) hydrogel in the presence of PDGF-BB were able to induce the activation of hMSCs, induce proliferation, spreading and migration (37). ➢ PDGF is known to synergistically enhance osteogenic differentiation through crosstalk between MEK- and PI3K/Akt-mediated signalling (66). PDGF alone, however, showed no signs of osteogenic differentiation in hMSCs (66).
Wnt3a	Cytokine	8.65E-10	ADM2,CTGF,DDIT4,EDN1,EGR2,EPHA5,FMOD,LBH,LEF1,LGR5,LRRC17,SFRP2,TMEM158,TNFRSF11B,TRIB3,VCAM1,WIF1	1,4	➢ Wnt3a signals through the Wnt/ β-catenin canonical pathway in regard to its importance in bone formation involving MSCs. ➢ Wnt3a-associated responsive promoter activation as a result of the Wnt signalling activation, depends on the MSC differentiation state. Wnt3a exposure has shown to inhibit MSC osteogenic differentiation, further decreasing matrix mineralisation and ALP activity (67).

					➢ Its overall effect drives an increase in cell number resulting from an enhanced proliferative activity and a decrease in apoptosis, particularly during the expansion of undifferentiated MSCs (68). ➢ Another study demonstrated the proliferative ability of Wnt3a on hMSCs while retaining pluripotency (36). ➢ Boland et al. have also shown that when osteogenically differentiated MSCs are treated with Wnt3a, it results in a decrease in osteoblastic marker gene expression. Canonical Wnt signalling functions in maintaining an undifferentiated, proliferating progenitor MSC population, whereas non-canonical Wnt signalling drive osteogenic differentiation via Wnt5a (68). To date, contradicting effects of Wnt3a are observed on MSC differentiation.
VEGF	Group	2.44E-09	ACKR3,ANGPTL4,BCL2A1,CDH1,CNN1,COL4A3,CRLF1,CXCL8,EDN1,ELN,FKBP5,HOPX,ITGA2,LEF1,NR4A2,OXTR,RGS2,STC1,THBD,TMEM158,TNFRSF11B,VCAM1	4,5	➢ VEGF belongs to the PDGF superfamily and is known to play a significant role in regulating angiogenesis and driving osteogenesis in bone repair and remodelling. ➢ VEGF has demonstrated its role in regulating hMSC differentiation potential. It controls the balance between osteogenesis in BM-MSCs via an intracrine mechanism but stimulates osteoclastogenesis and adipogenesis in a paracrine mechanism (69)(70). ➢ In conjunction with its effects on stem cell fate, VEGF has been shown to increase MSC proliferation significantly in a study carried out by (38). ➢ Profiled but not constant dose of VEGF had a significant impact on cell numbers. In comparison to the other growth factors tested as well in this study (IGF-1, FGF-2, BMP-2), VEGF demonstrated the highest proliferative rate in MSCs (38). ➢ According to this study, VEGF did not impact the differentiation potential and mineralization of MSCs. This is in agreement with a previous study confirming an increase in VEGF in the early proliferation stage of MSC during bone repair (38). ➢ The effects of 17β-estradiol on hMSC proliferation have shown to coincide with an increase in VEGF, both enhancing the cells proliferative potential (58). ➢ Furthermore, a separate study has demonstrated an inhibitory effect of VEGF on osteogenic commitment via the down regulation of BMP2 in rat MSCs, additionally attenuating MSCs differentiation potential (71).

TGF-β1	Growth Factor	2.44E-09	ACKR3,ANGPTL4,BCL2A1,CDH1,CNN1,COL4A3,CRLF1,CXCL8,EDN1,ELN,FKBP5,HOPX,ITGA2,LEF1,NR4A2,OXTR,RGS2,STC1,THBD,TMEM158,TNFRSF11B,VCAM1	1, 4, 5, 7	➤ As demonstrated by (72), TGF- β1 induces the translocation of β-catenin in MSCs in smad3- dependent manner, further inhibiting adipogenic differentiation (41). This pathway promotes the stimulation of MSC proliferation (41) and subsequently driving the inhibition of MSC osteogenic differentiation. ➤ A more recent study carried out by Yakota et al. have published findings supporting TGFβ's importance in regulating osteogenic differentiation. ➤ TGFβ plays a significant role in maintaining osteoblastic differentiation and proliferation, although inhibiting their maturation and mineralisation. This is induced via the activation of downstream intracellular effector molecules such as MAPKs (ERK pathway, p38 and JNK) and Smads (66).
FGF2	Growth Factor	1.06E-07	ANGPTL4,CCL20,CDH1,EDNRB,ELN,FGFR2,GREM1,HGF,IGF1,IGF2,LEF1,MMP1,NOG,NOV,NR4A2,SCD,TFPI,VCAM1	5	➤ According to Ahn et al. hMSCs cultured in the presence of FGF2 demonstrated enhanced growth and further maintained the cells pluripotent state during expansion. The associated MAPK signalling cascade, mediated by ERK, JNK and p38 protein kinase, primarily drives the cell's proliferative ability. ➤ In accordance to the study carried out by (39), JNK was found to play a major role in the FGF2-induced responses in regards to increasing the proliferation rate and survival of hMSCs but reducing their differentiation potential (39)(73).
IGF-1	Growth Factor	7.34E-09	BCL2A1,BIRC3,CDH1,CTGF,CXCL6,CXCL8,DDIT4,EDN1,EGR2,ELN,HGF,IGF1,IGF2,MMP1,NCF2,NOG,NUPR1,SCD,TGFBI,TNFRSF11B,VCAM1	4	➤ IGF-1 plays a critical role in bone formation and remodelling (42)(38). As confirmed by a number of studies, neutralising IGF-1 has shown to decrease ALP-2 activity and osteocalcin release from MSCs. Thus, demonstrating the essential role of IGF-1 in osteogenesis. ➤ On the contrary, Huang et al. have demonstrated the inhibitory effect of exogenous IGF-1 on MSC osteogenic differentiation. (38). ➤ Doorn et al investigated the effects of IGF-1 on hMSC proliferation and differentiation, confirming a concentration of 20 ng/mL demonstrating MSC proliferation. This study demonstrated the role of IGF-1 in inducing proliferation, expression of ALP and osteogenic gene expression of hMSC with a minimal effect of bone formation *in vivo* (74). ➤ These findings confirm the role IGF-1 in both bone formation and resorption.

Factors selected for the development of hPDC specific media. All 9 factors were shown to be primary hub genes in the study. P value of overlap determines whether there is a significant overlap between RNA Seq gene data set and the genes regulated by a specific upstream regulator (predicted regulated gene sets generated by IPA). The more

significant the overlap of an upstream regulator, the more the overlap of its target molecules that are expressed in the gene data set and predicted by IPA. The networks involved refer to the gene networks generated by IPA of which these selected factors are in association with. Please note: the 'Evidence to support selection of upstream regulators' is not a comprehensive literature review, rather it is evidence supporting a potential role in of each factor in proliferation, maintenance of viability and differentiation.

Supplementary Table 5

Growth Conditions	Initial Cell Density (cells/cm^2)	Density at Harvest (cells/cm^2) (mean ± S.E.M)	Population Doublings (mean ± S.E.M)	Population Doubling Time (Days) (mean ± S.E.M)
1% FBS	4,000	12,089 ± 1,060	1.57 ± 0.20	12.48 ± 1.4
10% FBS	4,000	22,444 ± 1,756*	2.48 ± 0.07***	2.02 ± 0.06***
PD-GFC	4,000	27,222 ± 2,946***	2.75 ± 0.17***	2.20 ± 0.14***

Data associated with a typical passage in each of the media formulations investigated in this study. (Data are presented as the mean ± S.E.M, Statistical analysis performed on all conditions relative to 1% FBS using one-way ANOVA, uncorrected Fischer's LSD; ***p<0.001; *p<0.05; n=3).